

**George Massey Tunnel
Replacement Project**



**BC JOBS
PLAN**



Ministry of
Transportation
and Infrastructure

Section 16.7

FRASER RIVER SALT WEDGE MODELLING

Technical Volume

George Massey Tunnel Replacement Project

This report has been produced for the Ministry of Transportation and Infrastructure regarding the George Massey Tunnel Replacement Project.

Subject: Modelling Study to Investigate the Impact of Removal of the George Massey Tunnel on the Salt Wedge [ISSUED FOR USE]

1.0 INTRODUCTION

The potential effect of the proposed removal of the George Massey Tunnel (Tunnel) on the hydrodynamics and the behaviour of the salt wedge in the Fraser River was evaluated using the proprietary three-dimensional hydrodynamic model, H3D.

Two cases were examined in this study: 1) the existing case with the Tunnel in place, and 2) the case without the Tunnel. The top of the Tunnel is at a depth approximately 12-13 m below geodetic datum and is slightly proud of the surrounding river bottom in the deepest part of the channel (Figure 1.1). For these simulations, it is assumed that after the Tunnel is removed or decommissioned, the river bathymetry will return to its natural configuration. Figure 1.2 shows the smoothed bathymetry in the river without the Tunnel, used as the initial case for modelling.

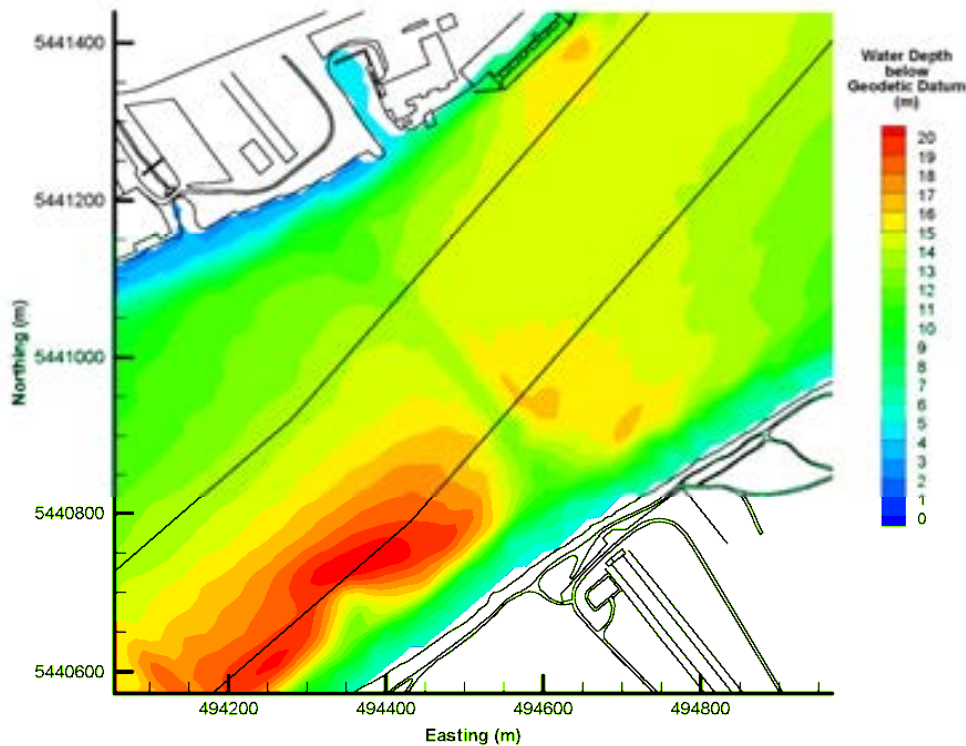


Figure 1.1: Existing Bathymetry near the George Massey Tunnel

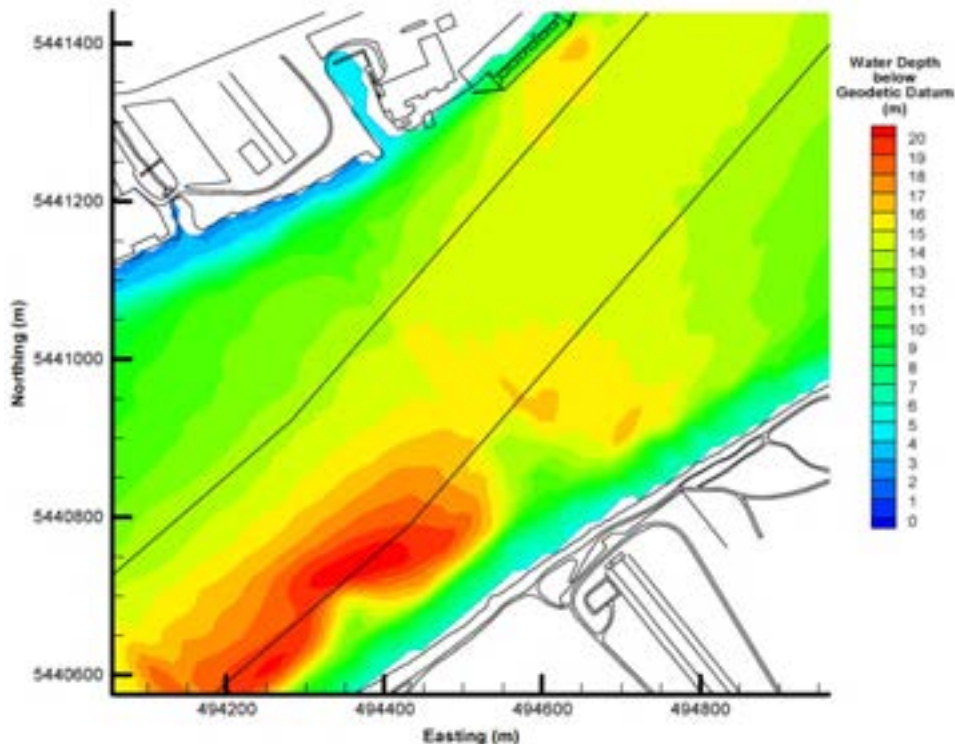


Figure 1.2: “Smoothed” Bathymetry without the Massey Tunnel

The lower reach of the Fraser River is an estuary with outflowing fresh river water on top of the saltier water intruding from the Strait of Georgia at the bottom, thereby forming a salt wedge. The behaviour of the salt wedge strongly depends on the tide and river flow: the salt wedge advances and retreats daily in accordance with the daily tidal pattern, while the seasonally-varying upstream extent of the salt wedge excursion depends on the flow rate in the Fraser River. Tidal characteristics in the river are that at high water, currents in the river are generally small, and become directed in the downstream direction as the water level falls, forming an ebb tide condition. Outflow velocities reach their peak values somewhat before low water, then start to decrease and then change to an up-river, flooding state on the rising tide.

During an ebbing tide, velocities in the river increases until about the time of low water, pushing the salt wedge downstream, and out of the river during high flows. On the other hand, during a flood tide the velocity changes to an upstream flow, offering less resistance to the upstream advancement the salt wedge, thereby allowing the salt wedge to migrate upstream. During the freshet period, the salt wedge retreats offshore of Sand Heads on the ebb tide and advances just past Steveston Island on the flood tide; whereas in the low flow period, it retreats to Steveston Island on the ebb tide, but can advance as far as Annacis Island (Thomson, 1981) on the flood tide.

The main interest regarding the salt wedge as identified by stakeholders is that removal of the Tunnel and the subsequent change of the bathymetry in the vicinity of the Tunnel alignment could provide an easier pathway for the salt wedge to migrate upstream, especially during low flow periods, and thereby reduce the period of time when low-salinity water is available for irrigation purposes. At present, the water intake of greatest interest, located just upstream of Tilbury Island, withdraws water from the Fraser River to supply nearby farmlands for agriculture and harvesting purposes, but only operates in the time windows during which the salt wedge is located sufficiently downstream from the intake location that the water being withdrawn meets an appropriate salinity criterion. Salinity

sensitivity in crops, expressed in terms of conductivity, starts at approximately 700 microsiemens per centimeter, or 700 $\mu\text{S}/\text{cm}$ and the salinity sensor at the No.6 Road pump station was set at 500 $\mu\text{S}/\text{cm}$ (from an article by Matthew Burrows). Water with salinity higher than the criterion value has the potential to cause damage to agricultural products and soil where it is applicable. In this study, the conductivity criterion value of 400 $\mu\text{S}/\text{cm}$ (0.34 parts per thousand (ppt) salinity) is used which is the threshold value for cranberry irrigation.

This report first presents the numerical model, and then provides validation data, based on a comparison of computed salinities versus those collected by a sensor at the intake.

Then key salinity parameters, include salinity levels, location of the salt wedge toe, and daily periods of water suitable for irrigation, with and without the Tunnel in place, are then extracted from model output and compared, in order to quantify the effect of removal of the Tunnel.

2.0 HYDRODYNAMIC MODELLING

2.1 Hydrodynamic Circulation Model

A detailed technical description of H3D is attached in Appendix A. The following is a brief summary.

H3D is a three-dimensional time-stepping numerical model which computes the three components of velocity (u,v,w) on a regular grid in three dimensions (x,y,z), as well as scalar fields such as salinity, temperature and contaminant concentrations. The model uses the Arakawa C-grid (Arakawa and Lamb, 1977) in space, and uses a two level semi-implicit scheme in the time domain.

H3D is an implementation of the numerical model developed by Backhaus (1983; 1985) which has had numerous applications to the European continental shelf, (Duwe et al., 1983; Backhaus and Meir Reimer, 1983), Arctic waters (Kampf and Backhaus, 1999; Backhaus and Kampf, 1999) and deep estuarine waters, (Stronach et al., 1993). Locally, H3D has been used to model the temperature structure of Okanagan Lake (Stronach et al., 2002), the transport of scalar contaminants in Okanagan Lake, (Wang and Stronach, 2005), sediment movement and scour / deposition in the Fraser River (published document), circulation and wave propagation in Seymour and Capilano dams, and salinity movement in the lower Fraser River. H3D forms the basis of the model developed by Saucier and co-workers for the Gulf of St. Lawrence (Saucier et al., 2003), and has been applied to the Gulf of Mexico (Rego et al., 2010).

2.2 Model Implementation

Study of the details of the hydrodynamics requires model nesting to better resolve small scale processes at and near the location of interest. The model used for this study operates in a double-nested configuration, shown in Figure 2.1.

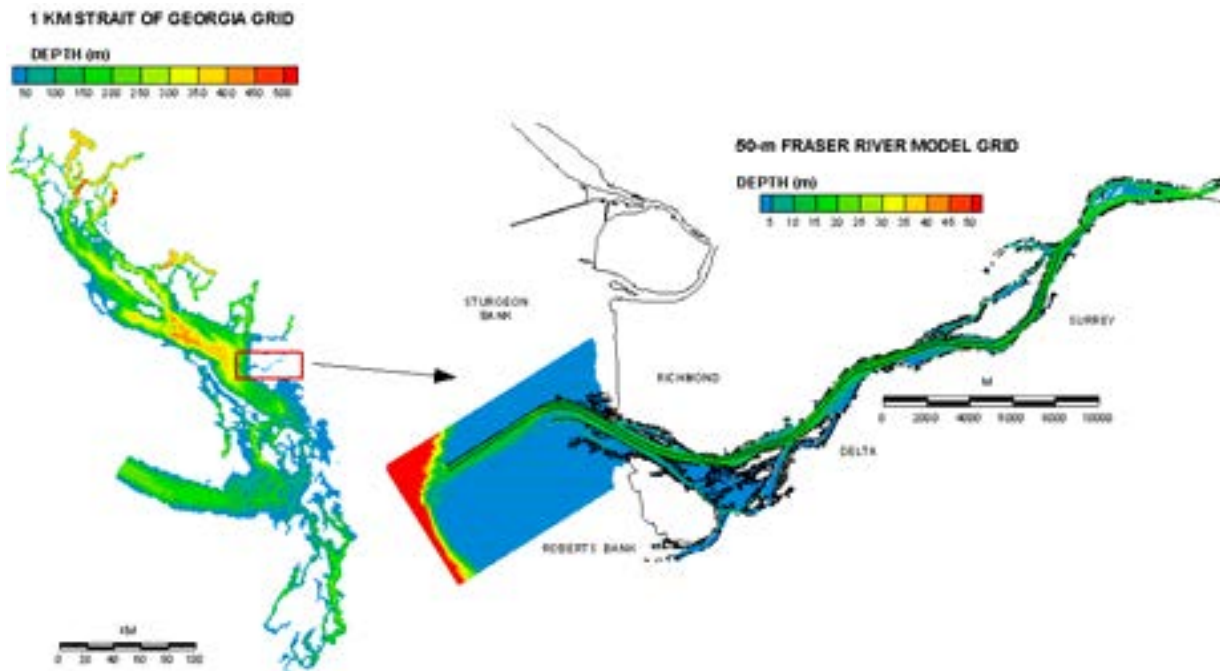


Figure 2.1: Model Nesting of Strait of Georgia and Fraser River Grids

The investigation of the behaviour of the salt wedge is done with a nominally 50-m resolution curvilinear model that spans the lower 41 km of the Fraser River, from Sand Heads to Port Mann Bridge. The model uses 50 m resolution in the along-channel direction, and 20 m in the cross-channel direction. This 50-m resolution model is in turn embedded within a nominally 1-km resolution model of the entire Strait of Georgia (SOG).

Both models simulate tidal, wind-driven and density-driven currents. Water level, velocity components and any scalar quantities output from the coarse grid model are passed on along the boundaries of the fine grid model and used to drive the finer-scale implementation of H3D. The fine-grid implementation provides the details of the effect of small-scale spatial variability in shorelines, depths and structures such as the tunnel cover.

The 1-km SOG model, driven by wind and density as well as tidal conditions along its open boundaries bordering the northern entrance to the Strait of Georgia and the western entrances to Juan de Fuca Strait includes a coarse representation of the Fraser River, extending upstream to km 41, with separate channels for the North Arm, the South Arm and Canoe Pass. At km 41, upstream of all salt wedge penetration, the model is dynamically coupled to a one-dimensional model of the Fraser River, extending to Hope. Tidal conditions are specified along the open boundaries of the 1-km SOG model.

The 50-m lower Fraser River model is driven at its upstream end by a flow boundary condition provided by the same dynamically-coupled one-dimensional model of the Fraser River that was also used for the 1-km model. At the downstream end, water levels and density profiles are obtained from the 1-km grid model, spatially interpolated from those cells of the 1-km grid model that correspond to the boundaries of the lower Fraser model.

The year 2011 was chosen for the modelling study as this is the year when bathymetry data collected from a bank-to-bank survey, from which the 50-m Fraser River model grid was constructed, is available; thus, the Fraser River flow rate in 2011 was used to drive the upstream boundary of the river model. The flow rate at the upstream boundary of the model is the combination of the flow rate at Hope and the estimated runoffs that report to the river downstream of Hope and upstream of Port Mann Bridge. Figure 2.2 shows the river flow rate at Hope in the year 2011. The model was run through the latter part of the fall season and beginning of winter season, from

November to January, when the flow rate at the Fraser River is low and the ability to withdraw freshwater from the river for harvesting is critical.

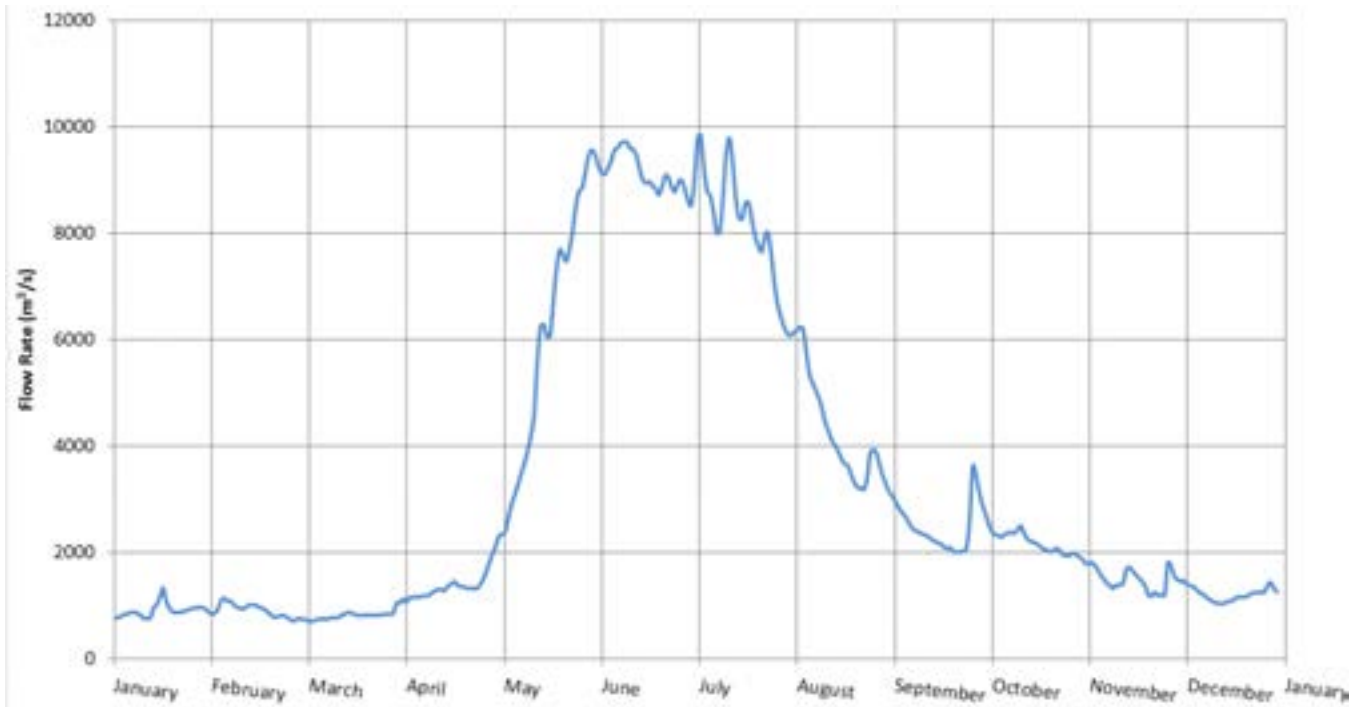


Figure 2.2: Fraser River Flow Rate at Hope in 2011

2.3 Model Validation

The model is validated against water level recorded at New Westminster, and against salinity data collected by a sensor installed at the intake near 8081 River Road, Delta. Data from a sensor that was mounted at 2 m depth from a floating platform is used for the comparison. Figure 2.3 shows comparison of salinity between observed and modelled values from November 3rd to 23rd. Also included in the figure are observed and modelled water levels for the same time period. Black lines show modelled values and red lines show observed values. Since the conductivity sensor cuts off at 5,500 $\mu\text{S}/\text{cm}$, the model results were similarly cut-off to facilitate comparison.

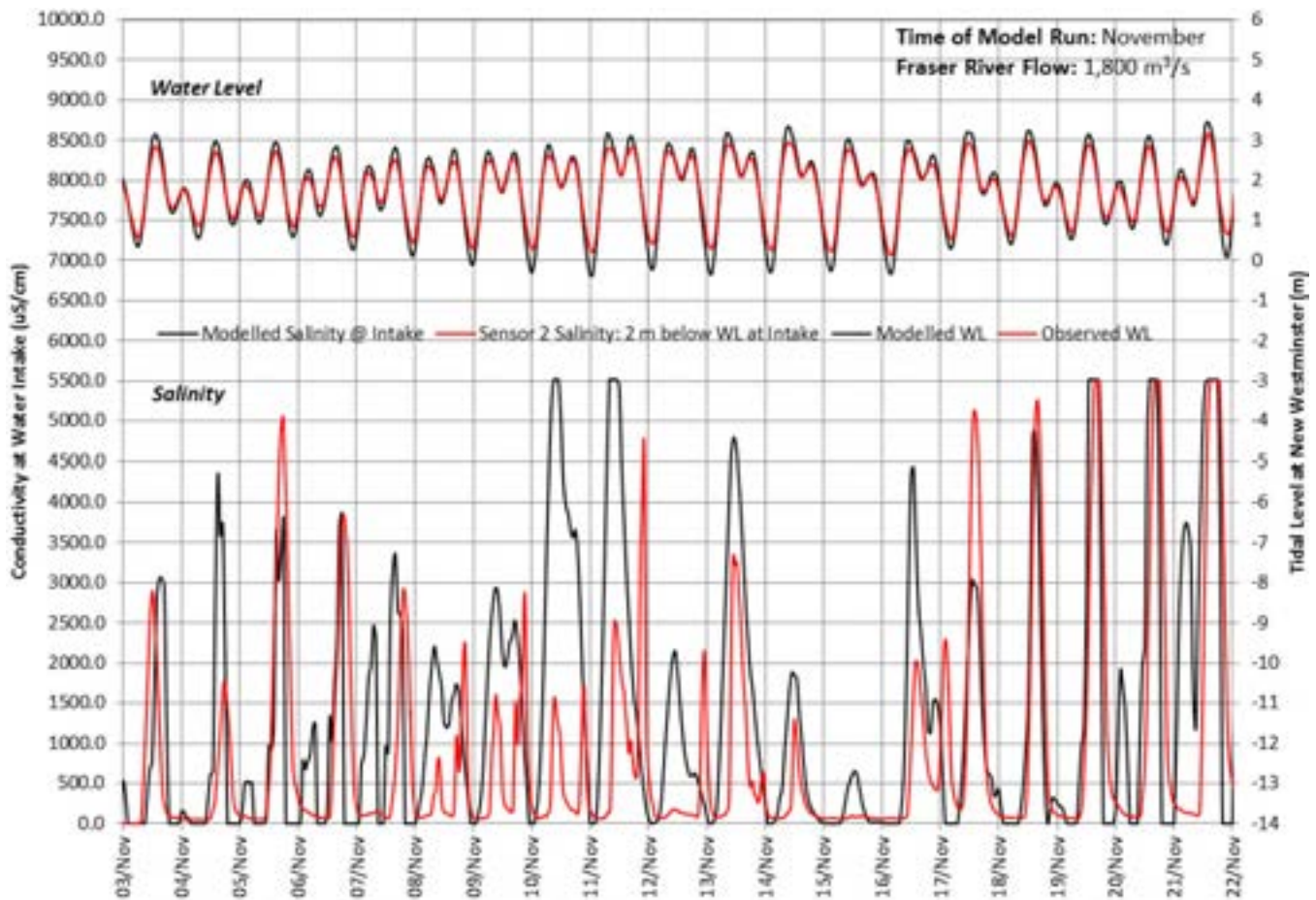


Figure 2.3: Comparison of Observed and Modelled Water Level and Salinity in the Fraser River

The model generally performs well predicting the trend of salinity and its variability on a daily time scale. In fact, the modelled salinities are frequently higher than observed, indicating that the model is conservative: it will under-predict the availability of water suitable for irrigation. However, the water intake is situated in a shallow area where complex processes controlling the movement of stratified flow might have contributed to the observed high variability and, sometimes, unpredictability in salinity at the intake. For example, the model almost always predicts an elevation of salinity during high tides when river flow is comparatively slower and water level in the river higher (for example, on November 7th); however, the sensor at the intake did not always detect such a salinity signal.

This behaviour can be partly understood by considering Figure 2.4, showing the map of salinity at the 2-m depth, on Nov 11 at 7 am, where the modelled result appears to deviate the most from the observed value. It can be seen that there is a high degree of spatial variability in the salinity field (at 2 m depth) in the vicinity of the intake. Salinity can vary from 3.5 ppt (4,500 $\mu\text{S}/\text{cm}$) to more than 5.0 ppt (6,500 $\mu\text{S}/\text{cm}$) near the intake in a matter of metres. Further analysis of model output demonstrates that there are two mechanisms for saline water to intrude onto the relatively shallow shelf on which the intake is located: either a selective withdrawal process, whereby saltier water is drawn up onto the bench from the adjacent deeper water (on both ebb and flood), or a process whereby the toe of the salt wedge rises to the surface upstream of the bench and then falls back partially onto the bench on the ebb tide.

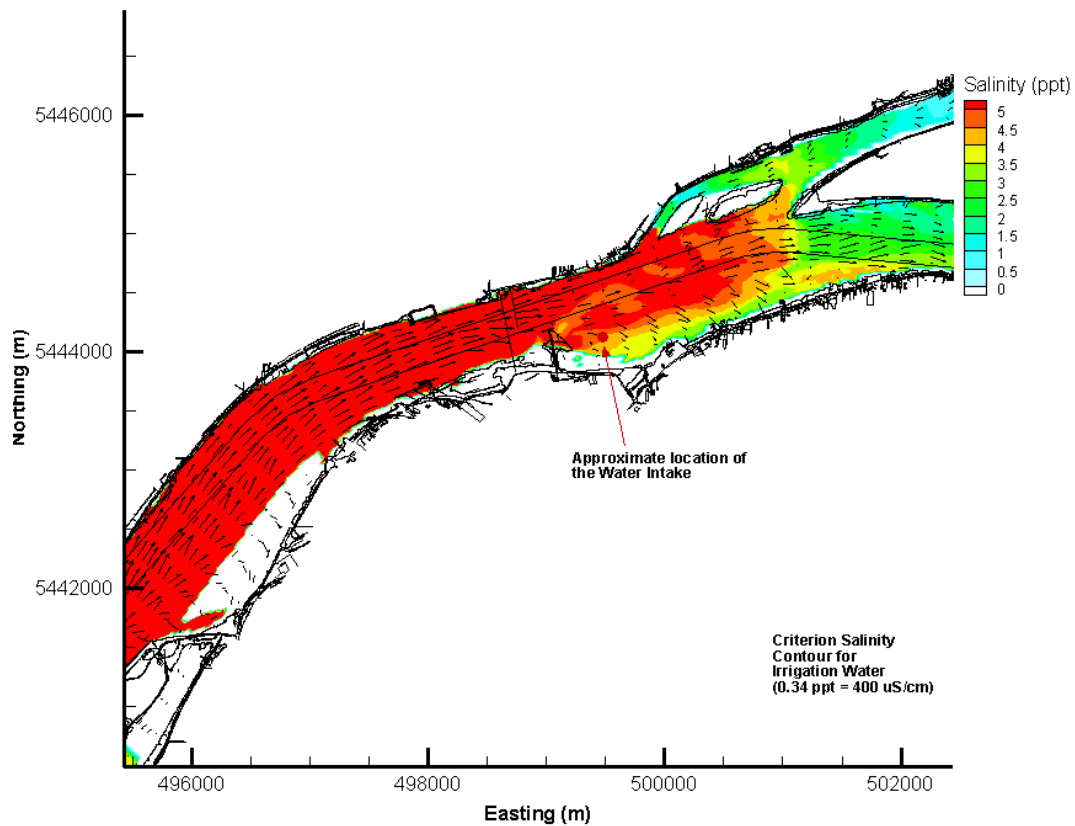


Figure 2.4: Snapshot of Salinity Contour at Intake Depth of 2m on November 11 at 7 am

Beside direct comparison of observed and modelled salinity, model validation can be considered from the perspective of water availability, which describes the onset and offset of salinity intrusion at the water intake and the time window within which river water can be safely withdrawn under the criterion salinity value of 0.35 ppt or 400 $\mu\text{S}/\text{cm}$. Figure 2.5 below compares the observed and modelled number of available hours per running 24 hours. The red line represents the observation and the black line represents the model results. The model, even though more conservative in general, was able to predict the overall trend in availability. Only a short period of record is presented, to facilitate visual comparison.

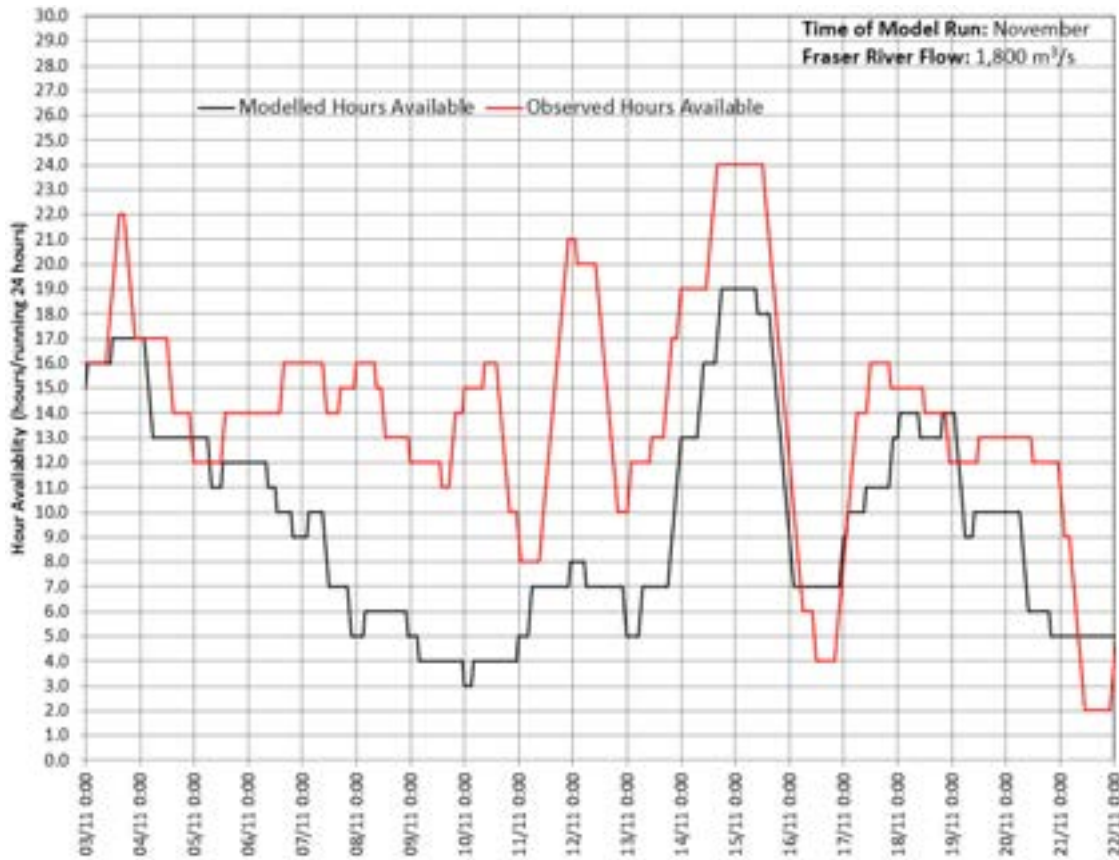


Figure 2.4: Comparison of Modelled and Observed Available Water Withdrawal Hours in November

The model, even though more conservative in general, was able to predict the overall trend in availability. The average number of hours available for water withdrawal in November is 14 hours per day based on observed salinity data, and 10 hours per day for the modelled case.

3.0 IMPACT OF TUNNEL REMOVAL

The hydrodynamic model simulations were run for the cases with and without the Tunnel. Although the model simulations presented in Section 2 did not always agree in detail with observations, the general characteristics are well-reproduced, and it is assumed that the differences in river hydrodynamics, with and without the Tunnel, will be captured by the model.

The effects of the absence of the Tunnel on the advancement of the salt wedge and on the salinity of the river water at the intake were assessed by comparing time-series of the salinity values at the water intake, as well as by comparing maps of salinity contours near the project location in the Fraser River. In this study, the focus is on the salt wedge behaviour during high tide periods, when the salt wedge migrates the furthest upstream.

This study focuses on the period between November and January during which the river flow decreases to a point where the salt wedge begins to exert effects on salinity in the water at the intake. The salt wedge remains mostly downstream of the Tunnel until November when the flow rate in the Fraser River drops to below 2,000 m³/s. The effects of the salt wedge become apparent during flood tide when the water level in the river is increasing and the flow speed is decreasing. Figure 3.1 shows the model results in terms of a time-series of salinity in mid-November at the intake. The black line represents the salinity at the intake for the case with Tunnel, and the green line

represents the case without the Tunnel, while the dotted blue line represents the salinity criterion for irrigation at 0.34 ppt(400 μ S/cm). Note the salinity difference between the two cases ranges between -0.1 ppt and 0.38 ppt, and, for most of the time, the absolute difference is less than 0.15 ppt.

The model was run continuously from November to January. Model results over only several tidal cycles were shown in the figures, however, to better illustrate visually the minute difference in the modelled salinity between the cases with and without the tunnel during the time of interest.

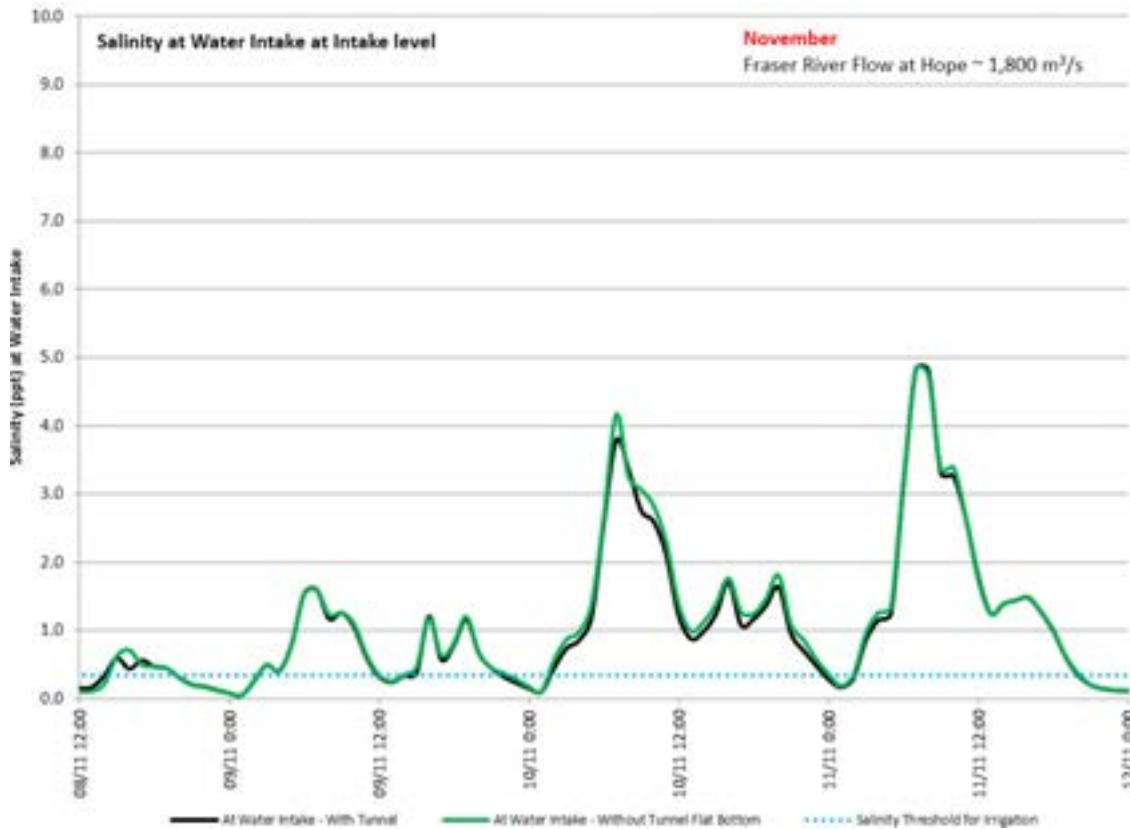


Figure 3.1: Modelled Intake Level Salinity at the Water Intake – November

Importantly, the modelling shows that at the location of the water intake, there is small difference between the salinity behaviour, in relative to the total salinity signal, with or without the Tunnel. The Root Mean Square (RMS) for the salinity signal is 1.36 ppt(1,760 μ S/cm), while the RMS of the salinity difference between the two cases is 0.11 ppt(143 μ S/cm), representing approximate 8% of the total salinity signal. The difference in salinity is greatest when salinities are high, and the water is unsuitable for irrigation.

Figure 3.2 shows, for the with-Tunnel case, a contour map of the salinity at the depth of the intake in the reach from the Tunnel to the water intake on November 13, 10 am during a high tide. Also included in the figure is an inset graph with the predicted (green line) and observed (black line) water levels at New Westminster; the blue and red lines represent the record high (4.66 m above CD) and low (0.42 m below CD) water levels measured at the location. Figure 3.3 shows the corresponding longitudinal sectional plot of salinity from Sand Heads (Km 0) to Annacis Island (Km 28). Figure 3.3 illustrates the upstream advance of the saline water, and that, consistent with Figure 3.2, surface salinities are around 2-3 ppt at the intake. Similarly, Figures 3.4 and 3.5 show the salinity contours for the without-Tunnel case. Figure 3.6 illustrates the two sets of plan view contours overlaid on one another to better illustrate the effect of the Tunnel removal on the salt wedge.

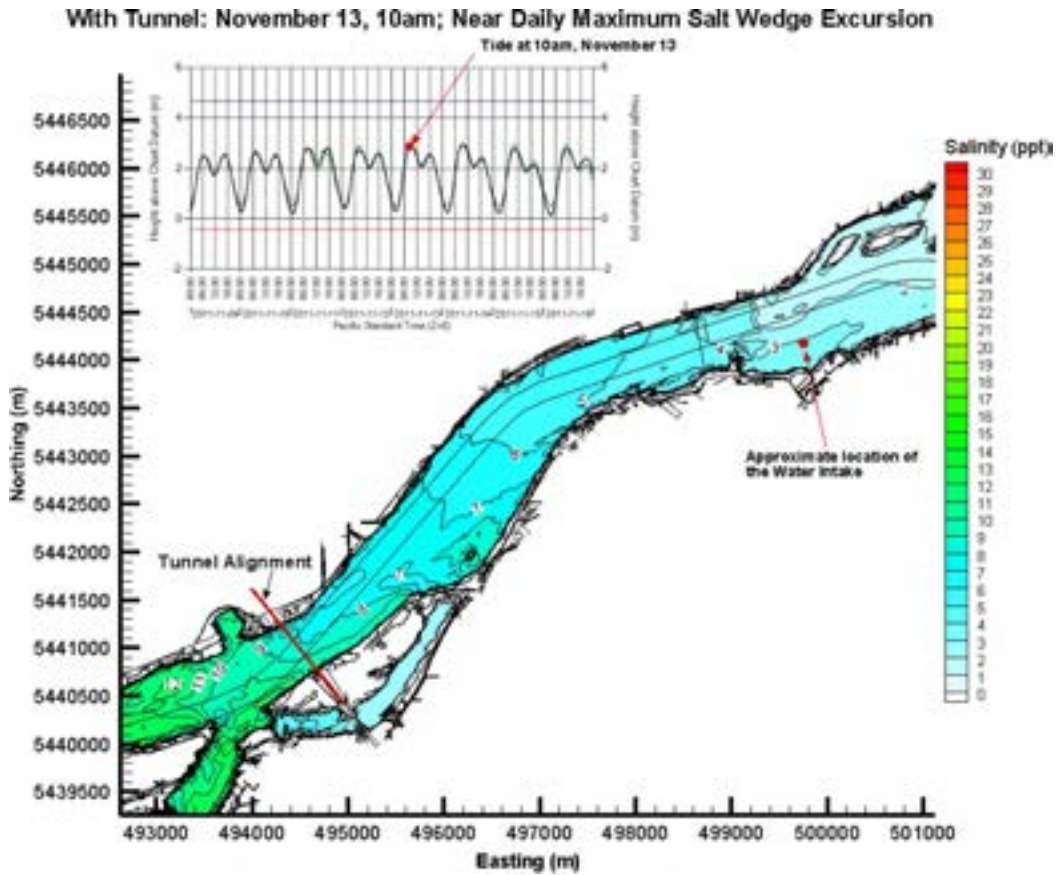


Figure 3.2: With Tunnel: Salinity Contour at Intake Level at High Tide, Nov 13, 2011 10:00 am

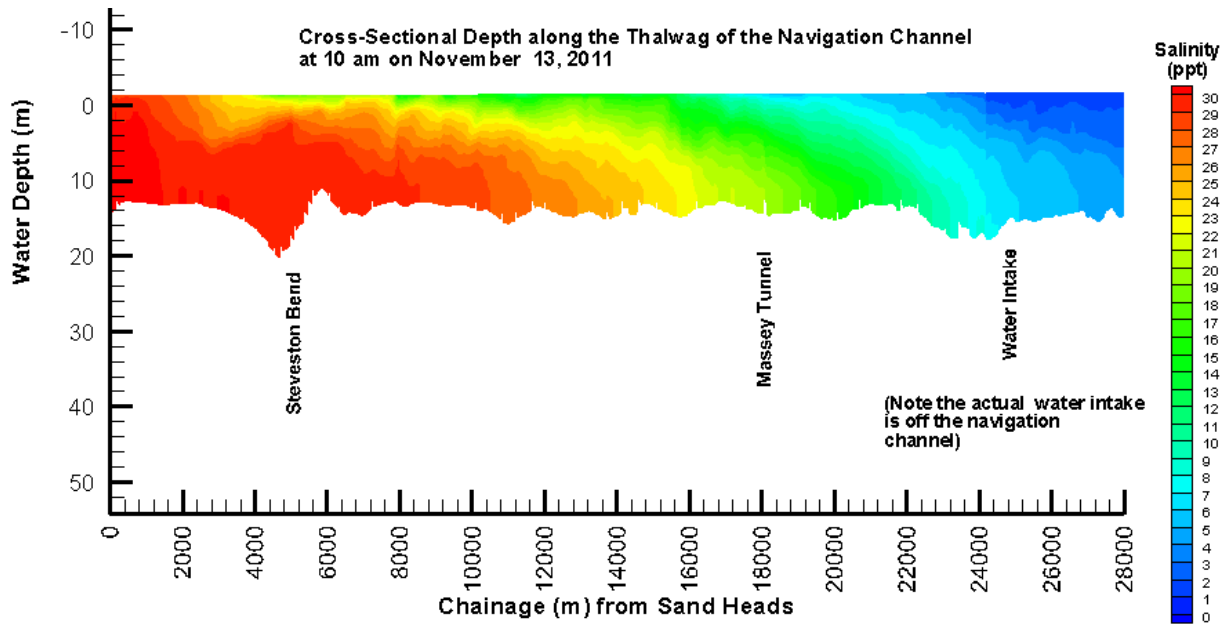


Figure 3.3: With Tunnel: Along-channel Salinity Contour at High Tide, Nov 13, 2011 10:00 am

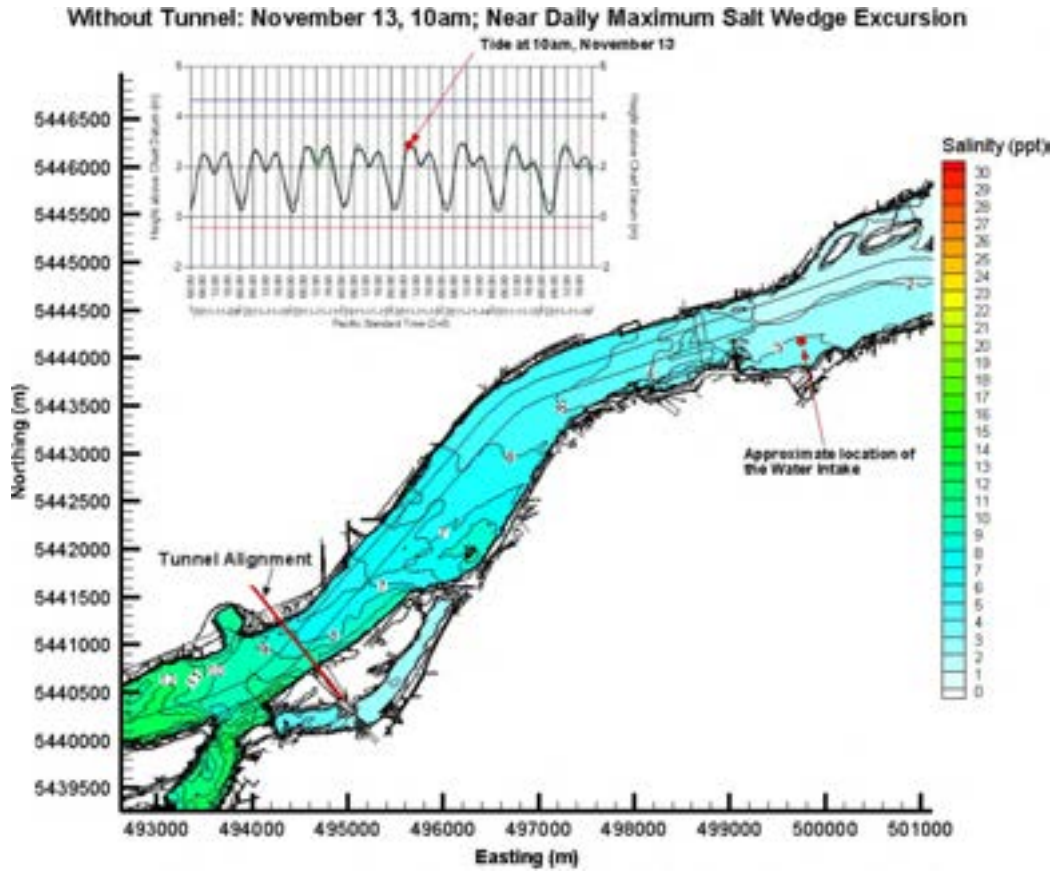


Figure 3.4: Without Tunnel: Salinity Contour at Intake Level at High Tide, Nov 13, 2011 10:00 am

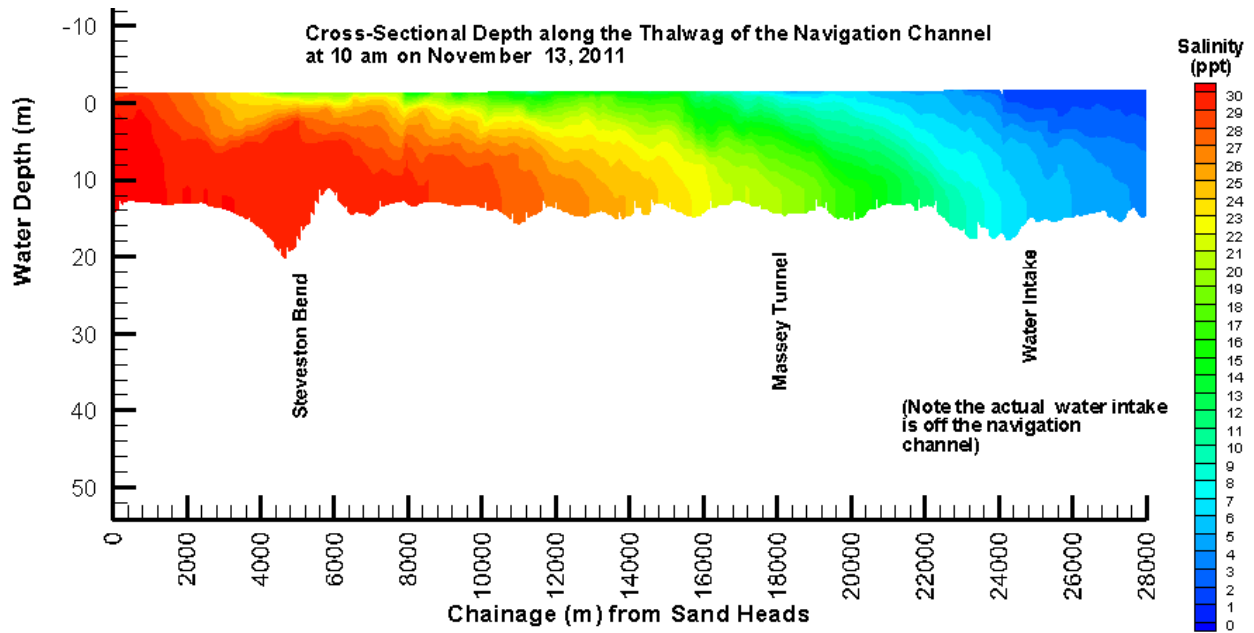


Figure 3.5: Without Tunnel: Along-channel Salinity Contour at High Tide, Nov 13, 2011 10:00 am

November 13, 10am; Near Daily Maximum Salt Wedge Excursion; Flow Rate = 1,800 m³/s

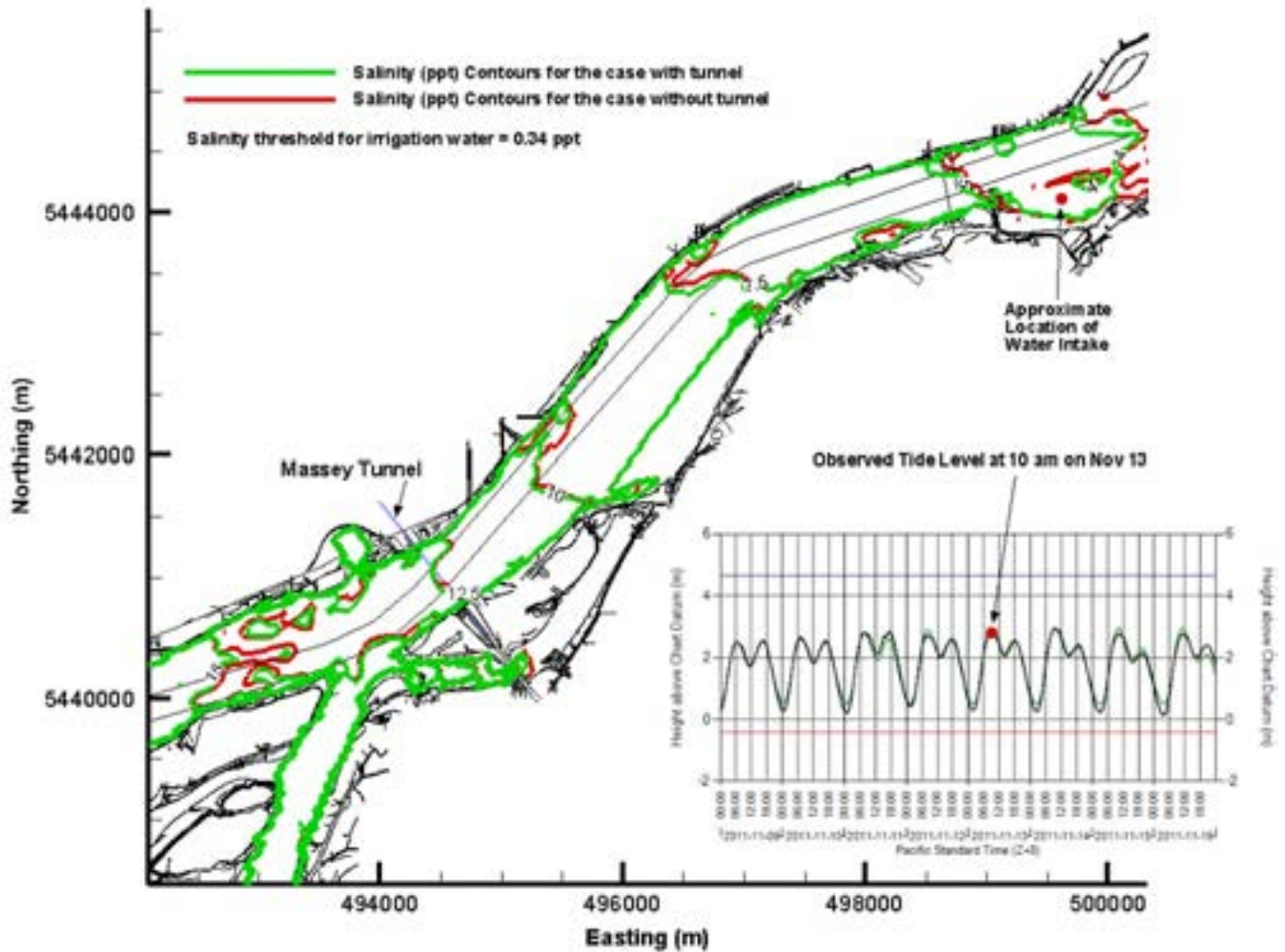


Figure 3.6: Overlaid Salinity Contours at Intake Level at High Tide, Nov 13, 2011 10:00 am

Figure 3.6 clearly indicates that the difference in the salt wedge behaviour between the two cases is generally small. The salt wedge without the Tunnel advances slightly further than in the case when the Tunnel is in place. The difference in salinity diminishes from downstream to upstream and there is only small difference in salinity at the location of the water intake (as illustrated in Figure 3.1).

Figures 3.7 and Figures 3.8 show similar time-series graphs for salinity at the water intake, but in December and January, respectively. Figure 3.9 and Figure 3.10 illustrate the overlaid salinity contour plots for December and January, respectively.

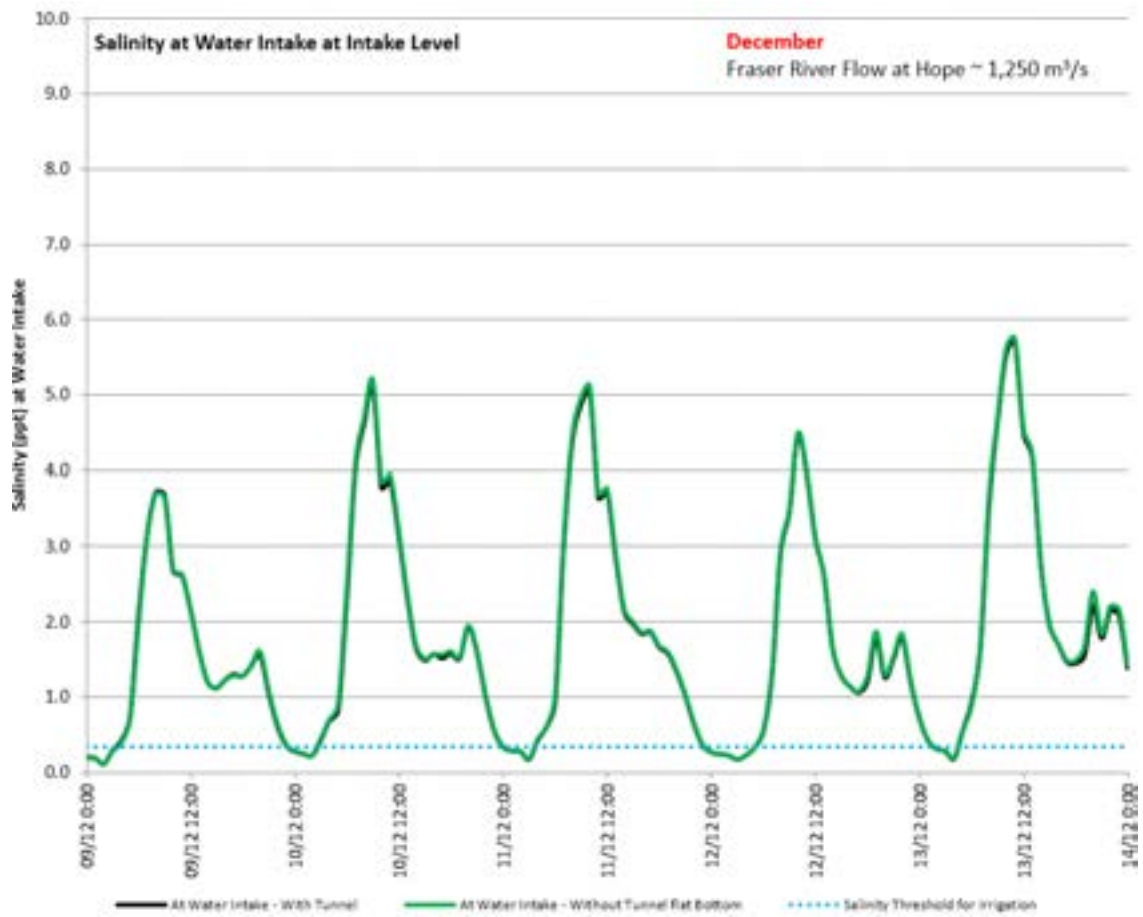


Figure 3.7: Modelled Intake Level Salinity at the Water Intake – December

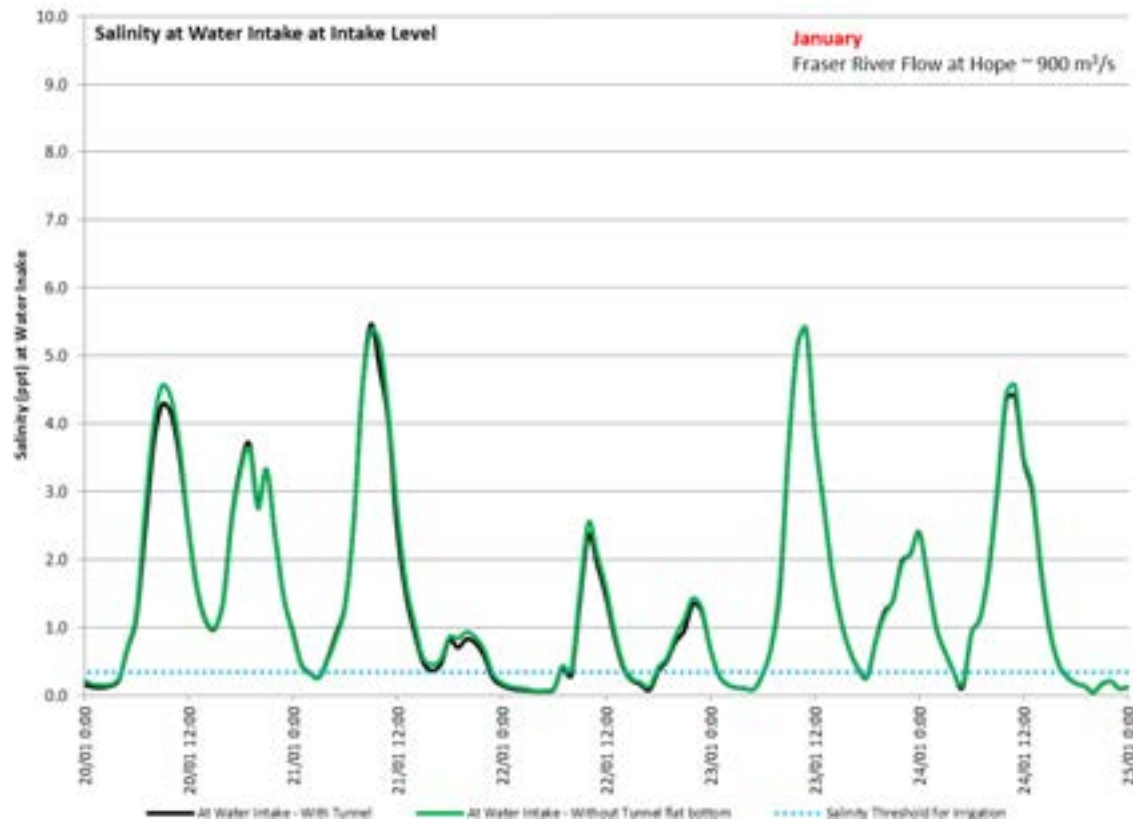


Figure 3.8: Time Series Modelled Salinity at the Water Intake – January

Figures 3.7 and 3.8 indicate that, similar to November, the difference in salinity is insignificant at the intake between the cases with and without the Tunnel. The RMS of the salinity difference is 0.04 ppt (57 $\mu\text{s/cm}$) for December, while the corresponding RMS for the salinity signal is 2.27 ppt (2,930 $\mu\text{s/cm}$), representing less than 2% of the total signal.

For January, the RMS of the salinity difference is 0.20 ppt (259 $\mu\text{S/cm}$), while the corresponding RMS for the salinity signal is 1.70 ppt or 2,200 $\mu\text{s/cm}$, representing approximately 12% of the total signal. The difference in salinity is rather large compared to the total signal; however, the largest salinity difference occurs during high tides when salinity reaches its peak, and the water is unsuitable for irrigation. Salinity, for the most part, remains very similar between the two cases. The difference in peak salinity value and the time window within which the salinity value exceeds the criterion salinity value is also insignificant.

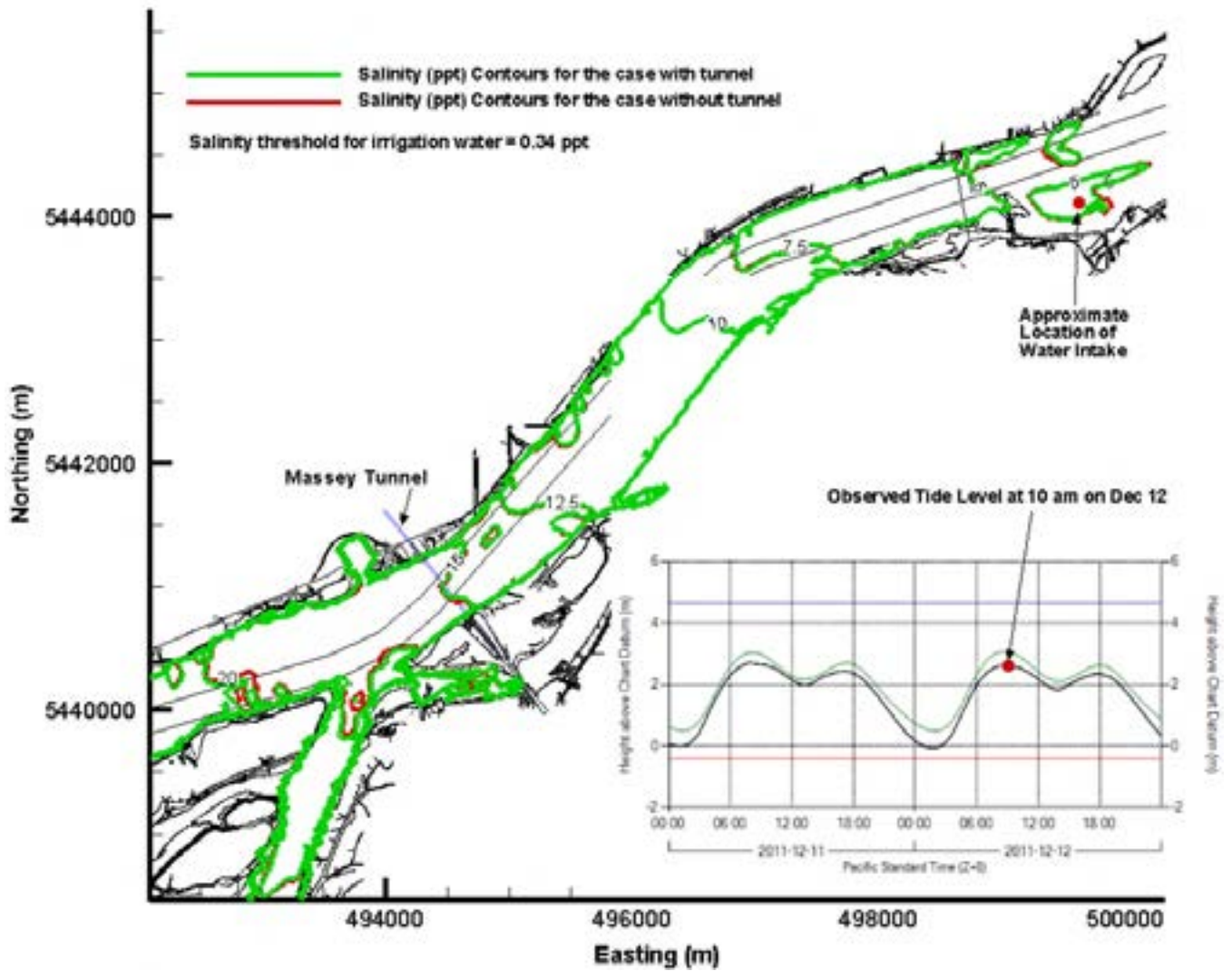


Figure 3.9: Overlaid Salinity Contours at Intake Level High Tide, December 12, 2011 10:00 am

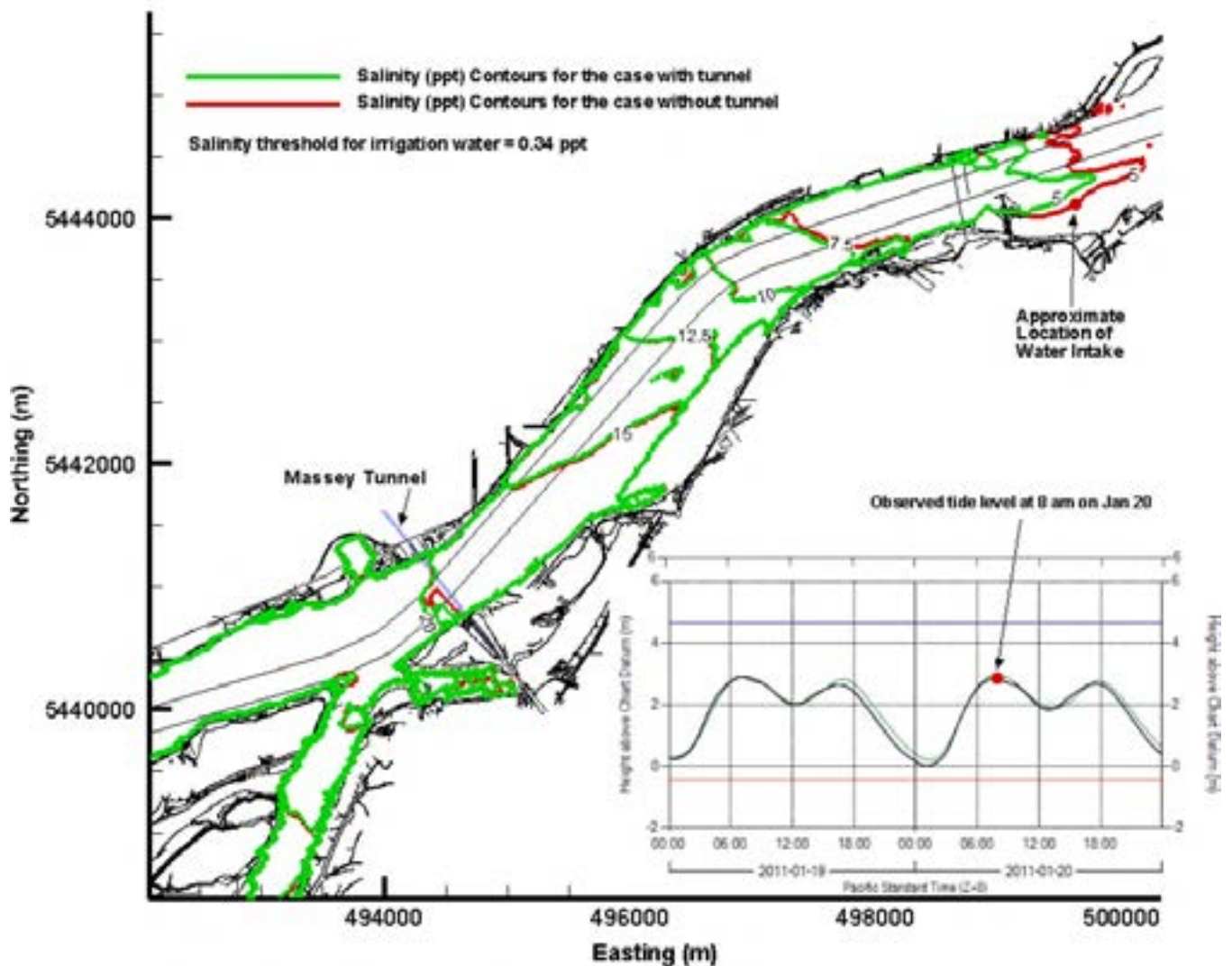


Figure 3.10: Overlaid Salinity Contours at Intake Level at High Tide, January 20, 2011 8:00 am

Figures 3.9 and 3.10 show that the extent of the salt wedge, as in November, behaves similarly between the cases with and without the Tunnel as can be seen by the largely overlapping salinity contours; the model does indicate a further advancement of the salt wedge when the Tunnel is removed as salinity contours can be found at locations mostly less than 50 m upstream in the case without the Tunnel

The small difference in the behaviour of the salt wedge in the pre- and post-removal cases is not unexpected. In the deepest part of the channel in which the salt wedge travels, the cross-channel ridge along the Tunnel alignment bounded by upstream and downstream scour degradation gives the impression that the Tunnel is proud of the surrounding river bottom to a similar height as that of the dynamic sand dunes formed in this part of the river. Figure 3.11 is a graphical excerpt from a 1995 report by Hay & Company (Hayco, 1995), showing the along-channel river bottom from the bathymetry survey in June of 1989 upstream of the tunnel (Massey Tunnel at km 18) and downstream of the intake at 8081 River Road (Intake at km 24). The x-axis is chainage distance measured from Sand Heads and y-axis is water depth. The natural variability of the river bottom in this area is a similar magnitude of, if not bigger than, the bottom associated with the presence of the Tunnel.

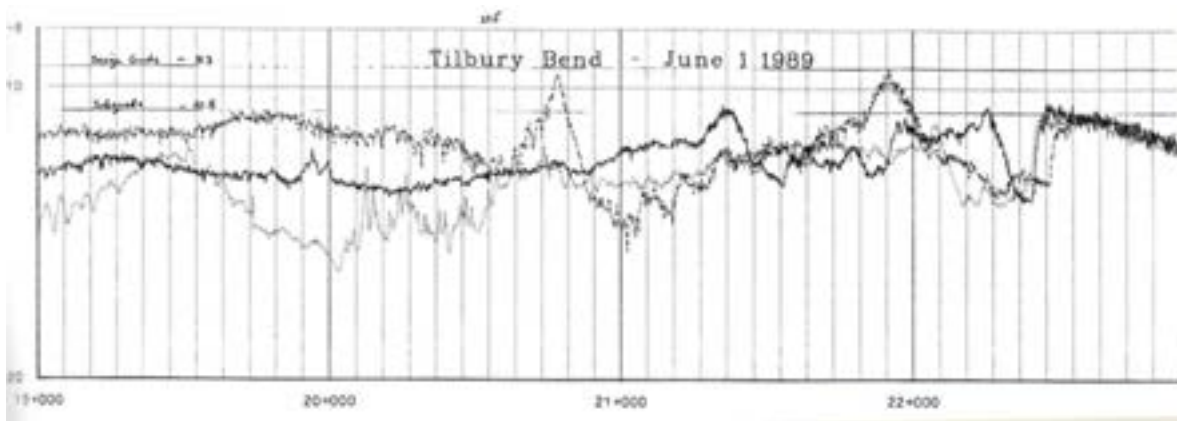


Figure 3.11: Bathymetry of Fraser River at Tilbury Bend upstream of the Tunnel (km 18) and downstream of the Intake (km 24) in June 1989

The river bottom along the Tunnel alignment, although not a migrating feature like dunes on the river bed, can be seen as one of these bottom elements in the river and thus, if considered individually, plays a very minor role in dictating the overall salt wedge behaviour.

4.0 CONCLUSIONS

The effects of the Tunnel removal on the hydrodynamics and salt wedge are summarized as follows:

- The proposed removal of the Tunnel will not affect the behaviour of the salt wedge.
- The effects of the Tunnel removal on the salt wedge diminishes in the upstream direction. While the salinity at the Tunnel alignment, for the case without the Tunnel, is slightly higher than that with the Tunnel, the time window during which the salinity in the water is higher than the criterion value is almost identical for the two cases at the location of the water intake.

The Tunnel does not act like a dam, which would have impeded the motion of water and the salt wedge in the river. The bathymetry footprint of the Tunnel is of no greater height and scale than the existing bathymetry features such as bed waves along other parts of the river.

5.0 CLOSURE

This report will be undertaken subject to the attached General Conditions, which will be incorporated into the report.

We trust this report meets your present requirements. If you have any questions or comments, please contact the undersigned.

Respectfully submitted,
Tetra Tech EBA Inc.



Prepared by:
Albert Leung, M.A.Sc., P.Eng., PE.
Hydrotechnical Engineer
Water and Marine Group
Direct Line: 778.945.5730
albert.leung@tetrattech.com

Reviewed by:
Jim Stronach, Ph.D., P.Eng.
Technical Specialist
Water and Marine Group
Direct Line: 778.945.5849
jim.stronach@tetrattech.com

/AL/JAS

REFERENCES

- Arakawa, A. and V.R. Lamb. 1977. Computational design of the basic dynamical processes of the UCLA general circulation model. *Methods in Computational Physics*, 17, 173-263.
- Ausenco Sandwell, BC Ministry of Environment - Climate change Adaption Guidelines for Sea Dikes and Coastal Flood hazard Land Use: Sea Dike Guidelines. 2011.
- Hay & Company Consultants Inc., Channel Maintenance Management Study, Lower Fraser Study. 1995.
- Thomson, R.E., *Oceanography of the British Columbia Coast*. 1981.
- Backhaus, J.O. 1983. A semi-implicit scheme for the shallow water equations for applications to shelf sea modelling. *Continental Shelf Research*, 2, 243-254.
- Backhaus, J.O. and E. Meir-Reimer. 1983. On seasonal circulation patterns in the North Sea. In: *North Sea Dynamics*, J. Sundermann and W. Lenz, editors. Springer-Verlag, Heidelberg, pp 63-84.
- Backhaus, J.O., and J. Kampf, 1999. Simulation of sub-mesoscale oceanic convection and ice-ocean interactions in the Greenland Sea. *Deep Sea Research Part II: Topical Studies in Oceanography*, 46, 1427-1455.
- Backhaus, J.O., 1985. A three-dimensional model for the simulation of shelf-sea dynamics. *Deutsche Hydrographische Zeitschrift*, 38, 165-187.
- Duwe, K.C., R.R. Hewer, and J.O. Backhaus. 1983. Results of a semi-implicit two-step method for the simulation of markedly non-linear flow in coastal seas. *Continental Shelf Research*, 2, 255-274.
- Kampf, J. and J.O. Backhaus, 1999. Ice-ocean interactions during shallow convection under conditions of steady winds: three-dimensional numerical studies. *Deep Sea Research Part II: Topical Studies in Oceanography*, 46, 1335-1355.
- Rego, J.L., E. Meselhe, J. Stronach and E. Habib. Numerical Modeling of the Mississippi-Atchafalaya Rivers' Sediment Transport and Fate: Considerations for Diversion Scenarios. *Journal of Coastal Research*, 26, 212-229.
- Saucier, F.J.; F. Roy, D. Gilbert, P. Pellerin and H. Ritchie. 2003. The formation of water masses and sea ice in the Gulf of St. Lawrence. *Journal of Geophysical Research*, 108 (C8): 3269–3289.
- Stronach, J.A., J.O. Backhaus, and T.S. Murty. 1993. An update on the numerical simulation of oceanographic processes in the waters between Vancouver Island and the mainland: the G8 model. *Oceanography and Marine Biology: an Annual Review*, 31, 1-86.
- Stronach, J.A., R.P. Mulligan, H. Soderholm, R. Draho, D Degen. 2002. Okanagan Lake Limnology: Helping to Improve Water Quality and Safety. *Innovation, Journal of the Association of Professional Engineers and Geoscientists of B.C.* November 2002.
- Wang, E and J.A. Stronach. 2005. Summerland Water Intake Feasibility Study. In "Water – Our Limiting Resource", Proceedings of a conference held in Kelowna Feb 23-25, 2005. BC Branch, Canadian Water Resources Association. pp. 256 – 269.

APPENDIX A

H3D TECHNICAL DESCRIPTION

APPENDIX A: H3D TECHNICAL DESCRIPTION

1.0 INTRODUCTION

H3D is an implementation of the numerical model developed by Backhaus (1983; 1985) which has had numerous applications to the European continental shelf, (Duwe et al., 1983; Backhaus and Meir Reimer, 1983), Arctic waters (Kampf and Backhaus, 1999; Backhaus and Kampf, 1999) and deep estuarine waters, (Stronach et al., 1993). Locally, H3D has been used to model the temperature structure of Okanagan Lake (Stronach et al., 2002), the transport of scalar contaminants in Okanagan Lake, (Wang and Stronach, 2005), sediment movement and scour / deposition in the Fraser River, circulation and wave propagation in Seymour and Capilano dams, and salinity movement in the lower Fraser River. H3D forms the basis of the model developed by Saucier and co-workers for the Gulf of St. Lawrence (Saucier et al., 2003), and has been applied to the Gulf of Mexico (Rego et al., 2010). H3D and its hydrocarbon transport and weathering module have been used in three recent environmental assessment applications currently before the appropriate regulatory agencies. H3D was used to simulate an existing and proposed reservoir for BC Hydro's Site C Clean Energy Project. Temperature, ice cover, and sedimentation characteristics of the proposed reservoir were predicted, supported by model validations in existing Dinosaur Reservoir. Two reports are available at the provincial Environmental Assessment Office. H3D was used to do oil spill modelling for the environmental and engineering assessments for the proposed Gateway project involving oil shipment out of Kitimat. The modelling work forms part of the information package submitted to the National Energy Board which is currently under review. Similarly, H3D was used to assess the fate of accidental fuel spills arising from a proposed jet fuel terminal in the Fraser River. This modelling work is part of the information package submitted to the provincial Environmental Assessment Office.

2.0 THEORETICAL BASIS

H3D is a three-dimensional time-stepping numerical model which computes the three components of velocity (u,v,w) on a regular grid in three dimensions (x,y,z), as well as scalar fields such as temperature and contaminant concentrations. The model uses the Arakawa C-grid (Arakawa and Lamb, 1977) in space, and uses a two level semi-implicit scheme in the time domain. H3D bears many similarities to the well-known Princeton Ocean Model (POM) (Blumberg and Mellor, 1987) in terms of the equations it solves, but differs in how the time-domain aspects are implemented. H3D uses a semi-implicit scheme, allowing relatively large time steps, and does not separately solve the internal and external models as POM does. It also uses a considerably simpler turbulence scheme in the vertical. These considerations combined allow H3D to execute complex problems relatively quickly.

The equations to be solved are:

Mass Conservation:

$$\frac{\partial u}{\partial x} + \frac{\partial v}{\partial y} + \frac{\partial w}{\partial z} = 0 \quad (\text{A1})$$

At the end of each timestep equation, (A1) is used to diagnostically determine the vertical component of velocity (w) once the two horizontal components of velocity (u and v) have been calculated by the model.

X-directed momentum:

$$\frac{\partial u}{\partial t} + u \frac{\partial u}{\partial x} + v \frac{\partial u}{\partial y} + w \frac{\partial u}{\partial z} + g \frac{\partial \eta}{\partial x} + \frac{1}{\rho_o} \frac{\partial}{\partial x} \int_z^\eta (\rho_w - \rho_o) g dz - f v \frac{\partial}{\partial x} A_H \frac{\partial u}{\partial x} - \frac{\partial}{\partial y} A_H \frac{\partial u}{\partial y} - \frac{\partial}{\partial z} A_V \frac{\partial u}{\partial z} = 0. \quad (\text{A2})$$

Y-directed momentum:

$$\frac{\partial v}{\partial t} + u \frac{\partial v}{\partial x} + v \frac{\partial v}{\partial y} + w \frac{\partial v}{\partial z} + g \frac{\partial \eta}{\partial y} + \frac{1}{\rho_o} \frac{\partial}{\partial y} \int_z^\eta (\rho_w - \rho_o) g dz + f u \frac{\partial}{\partial x} A_H \frac{\partial v}{\partial x} - \frac{\partial}{\partial y} A_H \frac{\partial v}{\partial y} - \frac{\partial}{\partial z} A_V \frac{\partial v}{\partial z} = 0. \quad (\text{A3})$$

Water surface elevation determined from the vertically-integrated continuity equation:

$$\frac{\partial \eta}{\partial t} = - \frac{\partial}{\partial x} \int_{-H}^\eta u dz - \frac{\partial}{\partial y} \int_{-H}^\eta v dz. \quad (\text{A4})$$

The effect of wind forcing introduced by means of the surface wind-stress boundary condition:

$$\left(A_V \frac{\partial u}{\partial z}, A_V \frac{\partial v}{\partial z} \right)_{z=\eta} = \frac{\rho_a}{\rho_w} C_{D,air} \bar{U}_{wind} \left| \bar{U}_{wind} \right|. \quad (\text{A5})$$

The effect of bottom friction introduced by the bottom boundary condition:

$$\left(A_V \frac{\partial u}{\partial z}, A_V \frac{\partial v}{\partial z} \right)_{z=-H} = K_{bottom} \bar{U}_{bottom} \left| \bar{U}_{bottom} \right|. \quad (\text{A6})$$

The bottom friction coefficient is usually understood to apply to currents at an elevation of one metre above the bottom. The bottom-most vector in H3D will, in general, be at a different elevation, i.e., at the midpoint of the lowest computational cell. H3D uses the 'law of the wall' to estimate the flow velocity at one metre above the bottom from the modelled near-bottom velocity.

The evolution of scalars, such as salinity, temperature, or suspended sediment, is given by the scalar transport/diffusion equation:

$$\frac{\partial S}{\partial t} + u \frac{\partial S}{\partial x} + v \frac{\partial S}{\partial y} + w \frac{\partial S}{\partial z} - \frac{\partial}{\partial x} N_H \frac{\partial S}{\partial x} - \frac{\partial}{\partial y} N_H \frac{\partial S}{\partial y} - \frac{\partial}{\partial z} N_V \frac{\partial S}{\partial z} = Q. \quad (\text{A7})$$

In the above equations:

$u(x,y,z,t)$: component of velocity in the x direction;

$v(x,y,z,t)$: component of velocity in the y direction;

$w(x,y,z,t)$: component of velocity in the z direction;

$S(x,y,z,t)$: scalar concentration;

$Q(x,y,z,t)$: source term for each scalar species

f : Coriolis parameter, determined by the earth's rotation and the local latitude;

$A_H(\partial u / \partial x, \partial u / \partial y, \partial v / \partial x, \partial v / \partial y)$: horizontal eddy viscosity;

$A_V(\partial u / \partial z, \partial v / \partial z, \partial \rho_{water} / \partial z)$: vertical eddy viscosity;

N_H : horizontal eddy diffusivity;

$N_V(\partial u / \partial z, \partial v / \partial z, \partial \rho_{water} / \partial z)$: vertical eddy diffusivity;

$C_{D,air}$: drag coefficient at the air-water interface;

$C_{D,bottom}$: drag coefficient at the water/sea bottom interface;

ρ_a : density of air;

$\rho_w(x,y,z,t)$: density of water;

ρ_o : reference density of water;

$\eta(x,y,t)$: water surface elevation;

$H(x,y)$: local depth of water.

The above equations are formally integrated over the small volumes defined by the computational grid, and a set of algebraic equations results, for which an appropriate time-stepping methodology must be found. Backhaus (1983, 1985) presents such a procedure, referred to as a semi-implicit method. The spatially-discretized version of the continuity equation is written as:

$$\eta^{(1)} = \eta^{(0)} - \alpha \frac{\Delta t}{\Delta l} (\delta_x U^{(1)} + \delta_y V^{(1)}) - (1 - \alpha) \frac{\Delta t}{\Delta l} (\delta_x U^{(0)} + \delta_y V^{(0)}) \quad (A8)$$

where superscript (0) and (1) refer to the present and the advanced time, δ_x and δ_y are spatial differencing operators, and U and V are vertically integrated velocities. The factor α represents an implicit weighting, which must be greater than 0.5 for numerical stability. $U^{(0)}$ and $V^{(0)}$ are known at the start of each computational cycle. $U^{(1)}$, and similarly $V^{(1)}$, can be expressed as:

$$U^{(1)} = U^{(0)} - g\alpha\Delta t\eta_x^{(1)} - g(1-\alpha)\Delta t\eta_x^{(0)} + \Delta tX^{(0)} \quad (A9)$$

where $X^{(0)}$ symbolically represents all other terms in the equation of motion for the u - or v -component, which are evaluated at time level (0): Coriolis force, internal pressure gradients, non-linear terms, and top and bottom stresses. When these expressions are substituted into the continuity equation (A4), after some further manipulations, there results an elliptic equation for $\delta_{i,k}$, the change in water level over one timestep at grid cell i,k (respectively the y and x directions):

$$\delta_{i,k} - (ce\delta_{i,k+1} + cw\delta_{i,k-1} + cn\delta_{i-1,k} + cs\delta_{i+1,k}) = Z_{i,k} \quad (\text{A10})$$

where ce , cw , cn , and cs are coefficients depending on local depths and the weighting factor (α), and $Z_{i,k}$ represents the sum of the divergence formed from velocities at time level (0) plus a weighted sum of adjacent water levels at time level (0).

Once equation (A10) is solved for $\delta_{i,k}$, the water level can be updated:

$$\eta_{i,k}^{(1)} = \eta_{i,k}^{(0)} + \delta_{i,k} \quad (\text{A11})$$

and equation (A9) can be completed.

At the end of each timestep, volume conservation is used to diagnostically compute the vertical velocity $w(j,i,k)$ from the two horizontal components u and v .

2.1 Vertical Grid Geometry

In the vertical, the levels near the surface are typically closely spaced to assist with resolving near-surface dynamics. In addition, the model is capable of dealing with relatively large excursions in overall water level as the water level rises and falls in response to varying inflows and outflows, by allowing the number of near-surface layers to change as the water level varies. That is, as water levels rise in a particular cell, successive layers above the original layer are turned on and become part of the computational mesh. Similarly, as water levels fall, layers are turned off. This procedure has proven to be quite robust, and allows for any reasonable vertical resolution in near-surface waters. When modelling thin river plumes in areas of large tidal range, the variable number of layers approach allows for much better control over vertical resolution than does the σ -coordinate method.

In addition to tides, the model is able to capture the important response, in terms of enhanced currents and vertical mixing, to wind-driven events. This is achieved by applying wind stress to each surface grid point on each time step. Vertical mixing in the model then re-distributes this horizontal momentum throughout the water column. Similarly, heat flux through the water surface is re-distributed by turbulence and currents in temperature simulations.

2.2 Turbulence Closure

Turbulence modelling is important in determining the correct distribution of velocity and scalars in the model. The diffusion coefficients for momentum (A_H and A_V) and scalars (N_H and N_V) at each computational cell are dependent on the level of turbulence at that point. H3D uses a shear-dependent turbulence formulation in the horizontal, (Smagorinsky, 1963). The basic form is:

$$A_H = A_{H0} dx dy \sqrt{\left(\frac{du}{dx}\right)^2 + \left(\frac{dv}{dy}\right)^2 + \frac{1}{2}\left(\frac{\partial v}{\partial x} + \frac{\partial u}{\partial y}\right)^2} \quad (\text{A12})$$

The parameter A_{H0} is a dimensionless tuning variable, and experience has shown it to lie in the range of 0.25 to 0.45 for most water bodies such as rivers, lakes and estuaries.

A shear and stratification dependent formulation, the Level 2 model of Mellor and Yamada (1982), is used for the vertical eddy diffusivity. The basic theory for the vertical viscosity formulation is taken from an early paper, Mellor and Durbin (1975). The evaluation of length scale is based on a methodology presented in Mellor and Yamada (1982).

For scalars, both horizontal and vertical eddy diffusivity are taken to be similar to their eddy viscosity counterparts, but scaled by a fixed ratio from the eddy viscosity values. Different ratios are used for the horizontal and vertical diffusivities. If data is available for calibration, these ratios can be adjusted based on comparisons between modelled and observed data. Otherwise, standard values based on experience with similar previously modelled water bodies are used. In a recent reservoir simulation, the ratio of vertical eddy diffusivity to vertical eddy viscosity was 0.75 and the ratio between horizontal eddy diffusivity and horizontal eddy viscosity was 1.0.

2.3 Scalar Transport

The scalar transport equation implements a form of the flux-corrected algorithm (Zalesak, 1979), in which all fluxes through the sides of each computational cell are first calculated using a second-order method. Although generally more accurate than a first order method, second order flux calculations can sometimes lead to unwanted high frequency oscillations in the numerical solution. To determine if such a situation is developing, the model examines each cell to see if the computed second order flux would cause a local minimum or maximum to develop. If so, then all fluxes into or out of that cell are replaced by first order fluxes, and the calculation is completed. As noted, the method is not a strict implementation of the Zalesak method, but is much faster and achieves very good performance with respect to propagation of a Gaussian distribution through a computational mesh. It does not propagate box-car distributions as well as the full Zalesak method, but achieves realistic simulations of the advection of scalars in lakes, rivers and estuaries, which is the goal of the model. This scheme as implemented is thus a good tradeoff between precision and execution time, important since in many situations, where more than one scalar is involved, the transport-diffusion algorithm can take up more than half the execution time.

2.4 Heat Flux at the Air-Water Interface

The contribution of heat flux to the evolution of the water temperature field can be schematized as:

$$\frac{dT}{dt} = \frac{\Delta Q}{\rho * c_p * h}$$

where ΔQ is the net heat flux per unit area retained in a particular layer, ρ is the density of water, c_p is the heat capacity of water and h is the layer thickness.

Heat flux at the air-water interface incorporates the following terms:

Q_{in} : incident short wave radiation. Generally, this is not known from direct observations. Generally, it is estimated from the cloud cover and opacity observations at nearby stations, a theoretical calculation of radiation at the top of the atmosphere based on the geometry of the earth/sun system, and an empirical adjustment based on radiation measurements at Vancouver Airport and UBC respectively for the period 1974-1977. This procedure has worked well for many water bodies, notably Okanagan Lake and the waters of

the north coast of British Columbia, in terms of allowing H3D to reproduce the observed temperature distributions in space and time. Values for albedo as a function of solar height are taken from Kondratyev (1972).

Q_{back} : net long wave radiation, calculated according to Gill (1982), involving the usual fourth power dependence on temperature, a factor of 0.985 to allow for the non-black body behaviour of the ocean, a factor depending on vapor pressure to allow for losses due to back radiation from moisture in the air, and a factor representing backscatter from clouds.

Q_L and Q_H : latent and sensible heat flux. Latent heat flux (Q_L) is the heat carried away by the process of evaporation of water. Sensible heat flux (Q_S) is driven by the air-water temperature difference and is similar to conduction, but assisted by turbulence in the air. Latent and sensible heat flux is described by:

$$Q_L = 1.32e^{-3} * L * windspeed * (q_{obs} - q_{sat}) * latent_factor$$

$$Q_S = 1.46e^{-3} * \rho_{air} * c_p * windspeed * (T_{air} - T_{water}) * sensible_factor$$

Where q_{obs} and q_{sat} are the observed and saturated specific humidities, T_{air} and T_{water} are the air and water temperatures, L is the latent heat of evaporation of water, and c_p is the heat capacity of water. ' $latent_factor$ ' and ' $sensible_factor$ ' are scaling factors introduced to account for local factors, and can be adjusted, when needed, to achieve better calibration of the model. Typically, the only adjustment is that $Sensible_factor$ is doubled when the air temperature is less than the water or ice surface temperature to account for increased turbulence in an unstable air column.

Light absorption in the water column. As light passes through the water column it is absorbed and the absorbed energy is a component of the energy balance that drives water temperature. H3D assumes that light attenuation follows an exponential decay law:

$$E(z) = E(z_0) * e^{-k*(z-z_0)}$$

The model computes the energy at the top and bottom of each layer and the difference is applied to the general heat equation in that layer. The extinction coefficient (k) is related to the Secchi depth (D_s) by

$$k = \frac{2.1}{D_s}$$

Temperature is treated like any other scalar as far as advection and diffusion are concerned. Heat flux at the water-sediment interface is not currently included in H3D.

2.5 Ice

The ice model is generally based on processes described in Patterson and Hamblin (1988). The ice cover is characterized by a thickness, a fraction of the cell covered, and an ice surface temperature. The temperature of the bottom of the ice is assumed to be the temperature of melting, usually 0° C. The strategy is to compute the differences in heat flux at the top and bottom of the ice layer and use this difference to determine the growth or decay rate and the change in temperature of the ice. The heat flux at

the bottom of the ice layer is dependent on lake temperature and water velocity. The heat flux at the top is dependent on meteorological processes and the surface temperature of the ice. The surface heat flux to the top of the ice sheet is calculated in a similar way as for open water, except that latent heat flux term (Q_L) also includes the heat of fusion. Albedo is also altered to account for ice/snow cover.

In order to start ice formation, once the surface water temperature drops below 3° C in a particular cell, a test ice layer of thickness 1 cm is initialized. If the test thickness melts in one time step, then the system cannot support ice cover in that cell at that time. If it survives, then the amount of ice in that cell is converted to a 1 cm thick region with coverage calculated from the mass of ice formed. In this way, a relatively robust start is made to ice formation.

The frictional interaction between the bottom of the ice and the immediately adjacent water is parameterized according to Nezhikhovskiy (1964).

2.6 Validation

Three validations of H3D's water level and temperature prediction skill are discussed below.

2.6.1 Strait of Georgia/Point Atkinson Tide: Wave Propagation

A fundamental concern with a circulation model such as H3D is how well it propagates waves, the carriers of information through the system. Figure A-1 presents results of a simulation of tides in the Strait of Georgia and Juan de Fuca Strait, with tidal elevations prescribed at the entrance to Juan de Fuca Strait and at a section north of Texada Island in the Strait of Georgia. The complex dynamics of the northern passes, such as Discovery Passage and Seymour Narrows, are thus avoided, allowing a test of H3D's wave propagation capabilities. The figure plots the modelled water level at Point Atkinson in red, and the observed water level in black. There is nearly perfect agreement, with the slight difference resulting from small storm surge events. This validation demonstrates that the selection of grid schematization (Arakawa C-grid) and the semi-implicit time-stepping approach have produced a system that can accurately propagate information through a water body.

2.6.2 Okanagan Lake Temperature Profiles

Obtaining good reproduction of the seasonally-evolving temperate structure of a lake indicates that the heat flux across the air-water interface is accurately parameterized and that the transport-diffusive processes operating in the water column are also accurately reproduced by the model. Figure A-2 presents a comparison of observed and computed temperature profiles at the northern end of Okanagan Lake near Vernon, in April, August, October and December of 1997. The agreement is very good as the model reproduced the transition from a well-mixed condition in the spring to the development of a strong thermocline in the summer, the deepening of the upper layer during the fall cooling period, and a return to isothermal conditions in winter. There is little doubt that H3D can compute accurate temperature distributions in water bodies, as long as adequate meteorological data is available. For this simulation, the meteorological data was obtained from Penticton Airport: winds, rotated to follow the thalweg of the valley; cloud cover, air temperature and relative humidity.

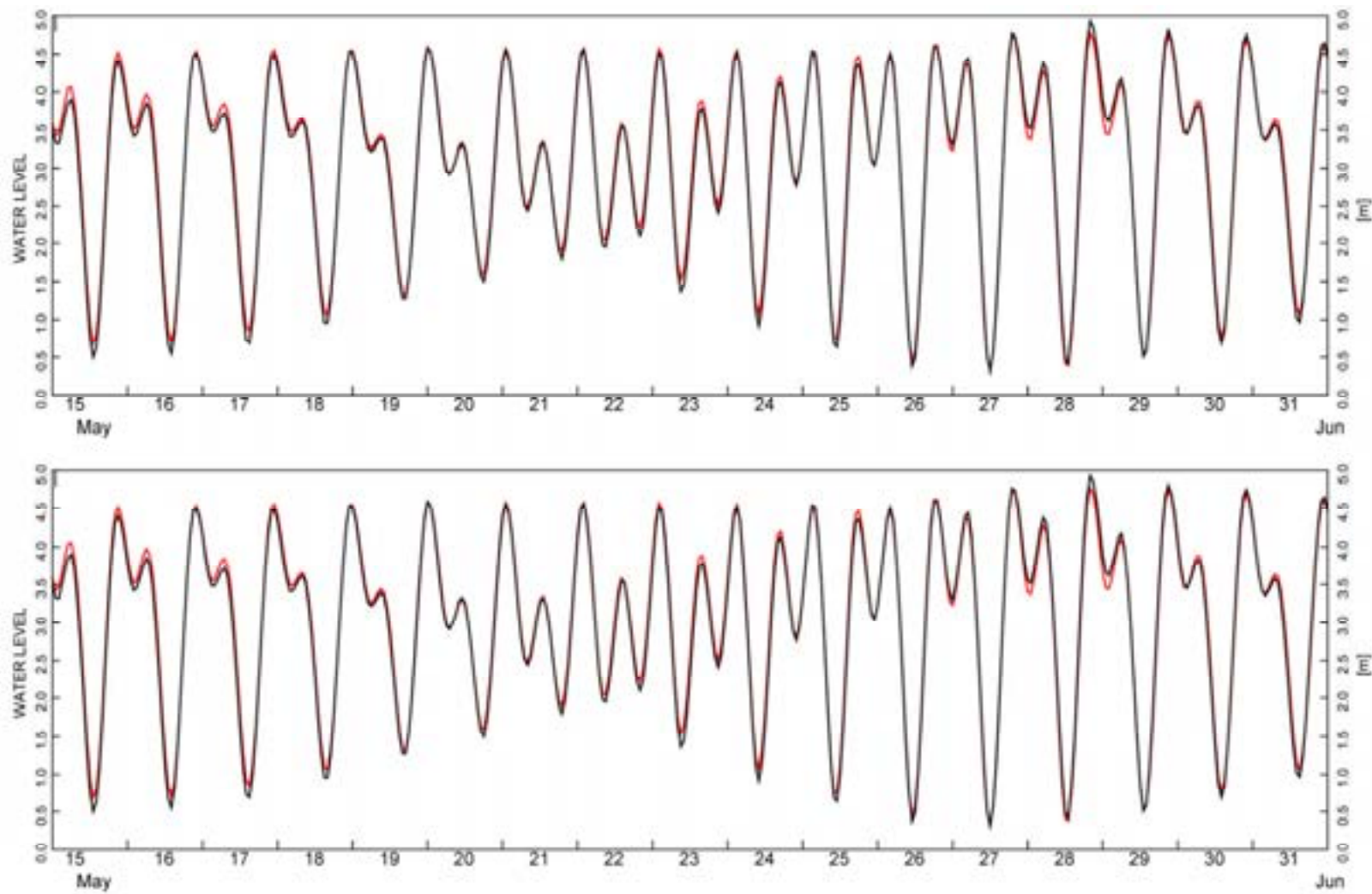
2.6.3 Thermistor Response: Okanagan Lake

Okanagan Lake is subject to significant fluctuations in the vertical thermal structure during the summer stratified period. Figure A-3 shows a temperature time-series at a site on the north side of the William R. Bennett Bridge which exhibits significant temperature excursions at periods of about 60 hours, or 2.5 days. Figure A-4 shows the modelled time series of temperature at three selected depths, 51 m, 21 m and 9 m. The occurrence and magnitude of the temperature fluctuations is generally predicted by the model, but the reproduction is not perfect: the occurrence and timing of the temperature events is quite good, but the modelled peaks appear to be generally somewhat broader in time. It was found that there were considerable differences in the simulated behaviour depending on whether winds at Kelowna Airport, which is situated in a side-valley, were included in the model or not. It is also clear that H3D can generally reproduce internal seiches in a lake, as long as adequate spatial resolution is used. This is particularly apparent when the coherent internal waves that propagate up and down the lake are examined in a longitudinal section, illustrated in two snapshots from a model simulation of such an event in Figure A-5.

REFERENCES

- Arakawa, A. and V.R. Lamb. 1977. Computational design of the basic dynamical processes of the UCLA general circulation model. *Methods in Computational Physics*, 17, 173-263.
- Backhaus, J.O. 1983. A semi-implicit scheme for the shallow water equations for applications to shelf sea modelling. *Continental Shelf Research*, 2, 243-254.
- Backhaus, J.O. and E. Meir-Reimer. 1983. On seasonal circulation patterns in the North Sea. In: *North Sea Dynamics*, J. Sundermann and W. Lenz, editors. Springer-Verlag, Heidelberg, pp 63-84.
- Backhaus, J.O., and J. Kampf, 1999. Simulation of sub-mesoscale oceanic convection and ice-ocean interactions in the Greenland Sea. *Deep Sea Research Part II: Topical Studies in Oceanography*, 46, 1427-1455.
- Backhaus, J.O., 1985. A three-dimensional model for the simulation of shelf-sea dynamics. *Deutsche Hydrographische Zeitschrift*, 38, 165-187.
- Blumberg, A. F. and G. L. Mellor, A description of a three-dimensional coastal ocean circulation model, In *Three-Dimensional Coastal Ocean Models*, N. S. Heaps, editor. American Geophysical Union, Washington, DC, 1987, pp 1-16.
- Duwe, K.C., R.R. Hewer, and J.O. Backhaus. 1983. Results of a semi-implicit two-step method for the simulation of markedly non-linear flow in coastal seas. *Continental Shelf Research*, 2, 255-274.
- Friehe C.A. and K.F. Schmitt, 1976. Parameterization of air-sea interface fluxes of sensible heat and moisture by the bulk aerodynamic formulas. *Journal of Physical Oceanography*. 76:801-805.
- Kampf, J. and J.O Backhaus, 1999. Ice-ocean interactions during shallow convection under conditions of steady winds: three-dimensional numerical studies. *Deep Sea Research Part II: Topical Studies in Oceanography*, 46, 1335-1355.
- Kondratyev, K.Y., 1972. *Radiation Processes in the Atmosphere*, WMO No. 309,.

- Mellor, G.L. and P.A. Durbin. 1975. The structure and dynamics of the ocean surface mixed layer. *Journal of Physical Oceanography*, 5, 718-728.
- Mellor, G.L. and T. Yamada. 1982. Development of a turbulence closure model for geophysical fluid problems. *Reviews of Geophysics and Space Physics*, 20, 851-875.
- Nezhikhovskiy, R.A. 1964. Coefficients of roughness of bottom surface of slush-ice cover. *Soviet Hydrology: Selected Papers*, 2, 127-150.
- Rego, J.L., E. Meselhe, J. Stronach and E. Habib. Numerical Modeling of the Mississippi-Atchafalaya Rivers' Sediment Transport and Fate: Considerations for Diversion Scenarios. *Journal of Coastal Research*, 26, 212-229.
- Saucier, F.J.; F. Roy, D. Gilbert, P. Pellerin and H. Ritchie. 2003. The formation of water masses and sea ice in the Gulf of St. Lawrence. *Journal of Geophysical Research*, 108 (C8): 3269–3289.
- Smagorinsky, J. 1963. General circulation experiments with primitive equations I. The basic experiment. *Monthly Weather Review*, 91, 91-164.
- Stronach, J.A., J.O. Backhaus, and T.S. Murty. 1993. An update on the numerical simulation of oceanographic processes in the waters between Vancouver Island and the mainland: the G8 model. *Oceanography and Marine Biology: an Annual Review*, 31, 1-86.
- Stronach, J.A., R.P. Mulligan, H. Soderholm, R. Draho, D Degen. 2002. Okanagan Lake Limnology: Helping to Improve Water Quality and Safety. *Innovation, Journal of the Association of Professional Engineers and Geoscientists of B.C.* November 2002.
- Wang, E and J.A. Stronach. 2005. Summerland Water Intake Feasibility Study. In "Water – Our Limiting Resource", Proceedings of a conference held in Kelowna Feb 23-25, 2005. BC Branch, Canadian Water Resources Association. pp. 256 – 269.
- Zalesak, S.T. 1979. Fully multidimensional flux-corrected transport algorithms for fluids. *Journal of Computational Physics*, 31, 335-362.



LEGEND

- Solid lines represent observed profiles
- Dash lines represent modelled profiles

NOTES

STATUS

CLIENT

-



H3D TECHNICAL DESCRIPTION

**H3D Validation
Tidal Reproduction**

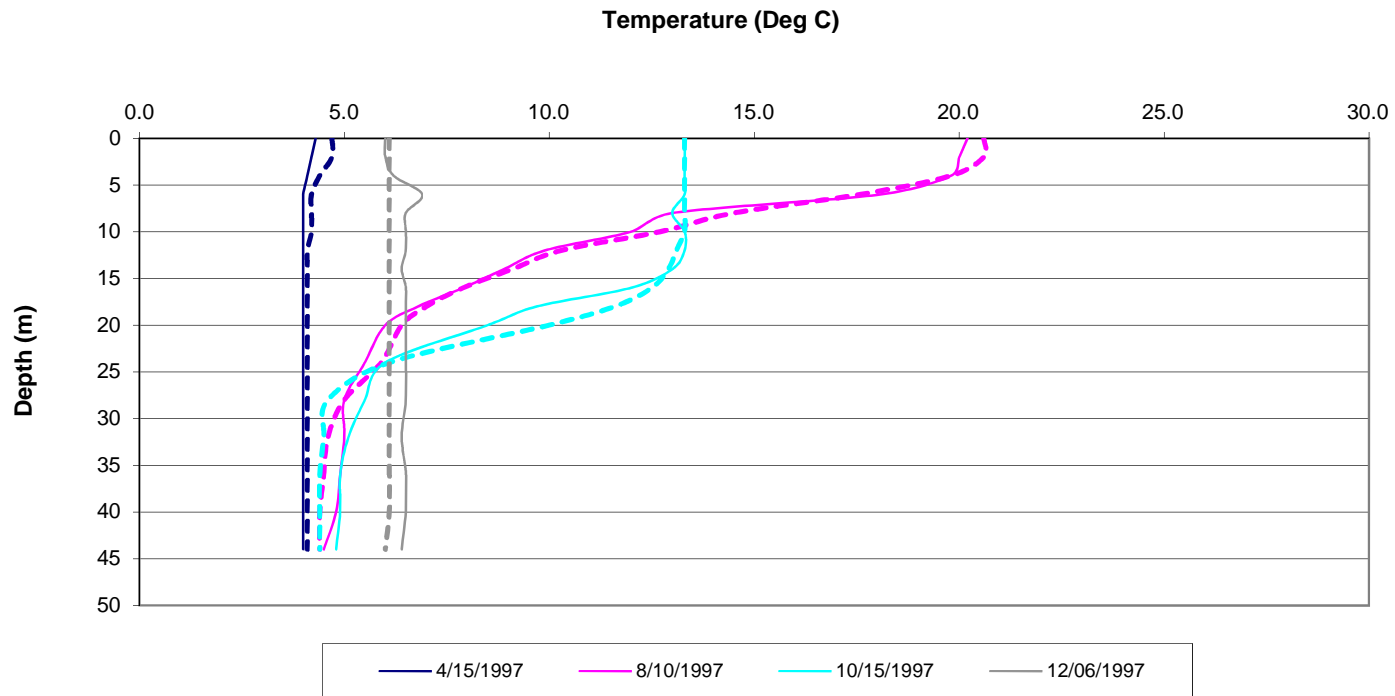
PROJECT NO.
V132

OFFICE
EBA-VANC

DWN AL	CKD JAS	APVD JAS	REV 001
------------------	-------------------	--------------------	-------------------

DATE
August 2011

Figure A-1



LEGEND

- Solid lines represent observed profiles
- Dash lines represent modelled profiles

NOTES

STATUS
ISSUED FOR USE

CLIENT

-

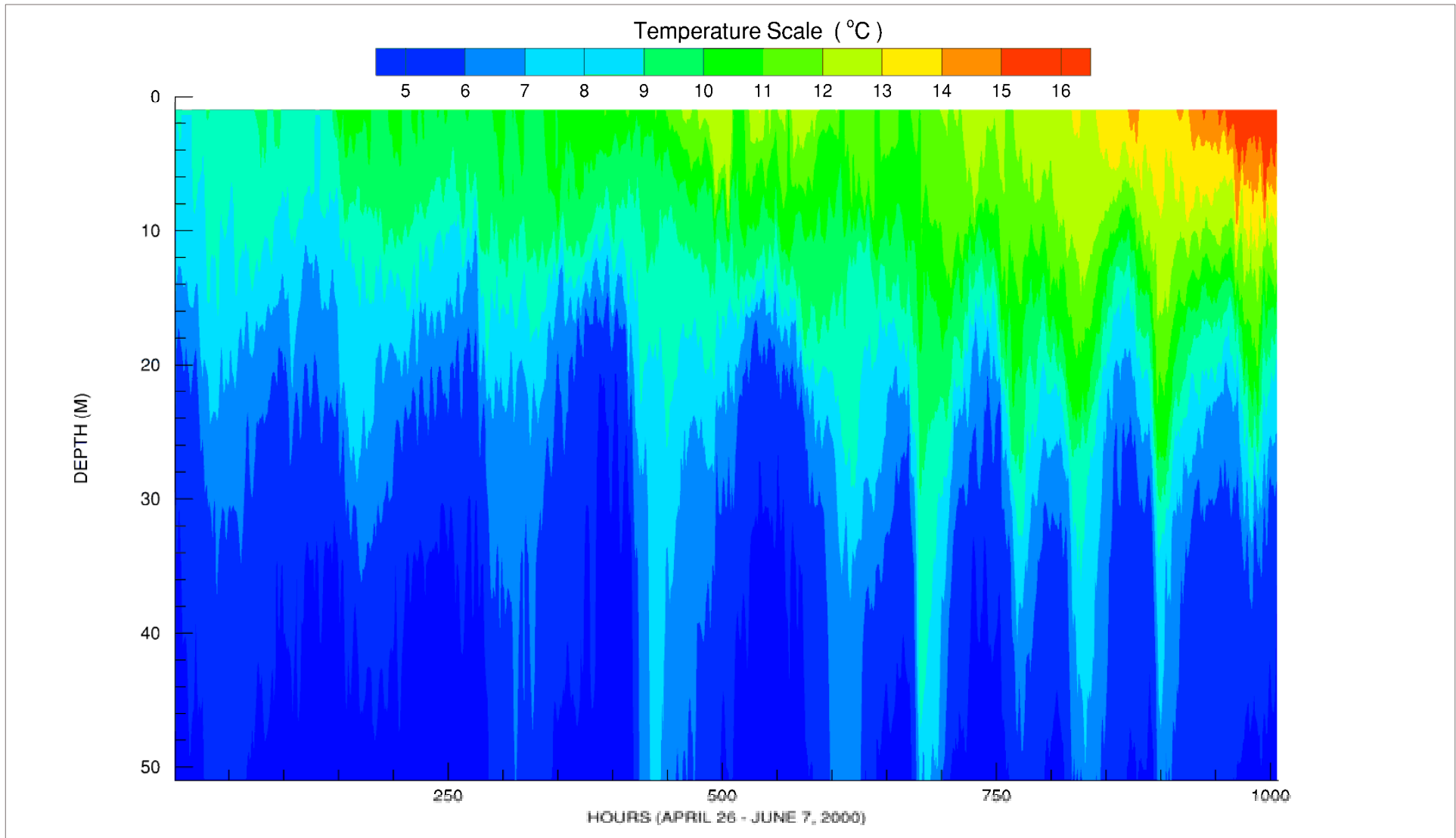


H3D TECHNICAL DESCRIPTION

**H3D Validation
Comparison of Observed and Modelled
Temperature Profiles at Vernon**

PROJECT NO. V132	DWN AL	CKD JAS	APVD JAS	REV 001
OFFICE EBA-VANC	DATE August , 2011			

Figure A-2



LEGEND

NOTES

CLIENT

H3D TECHNICAL DESCRIPTION

**H3D VALIDATION
SEICHES IN OKANAGAN LAKE
(OBSERVED DATA)**

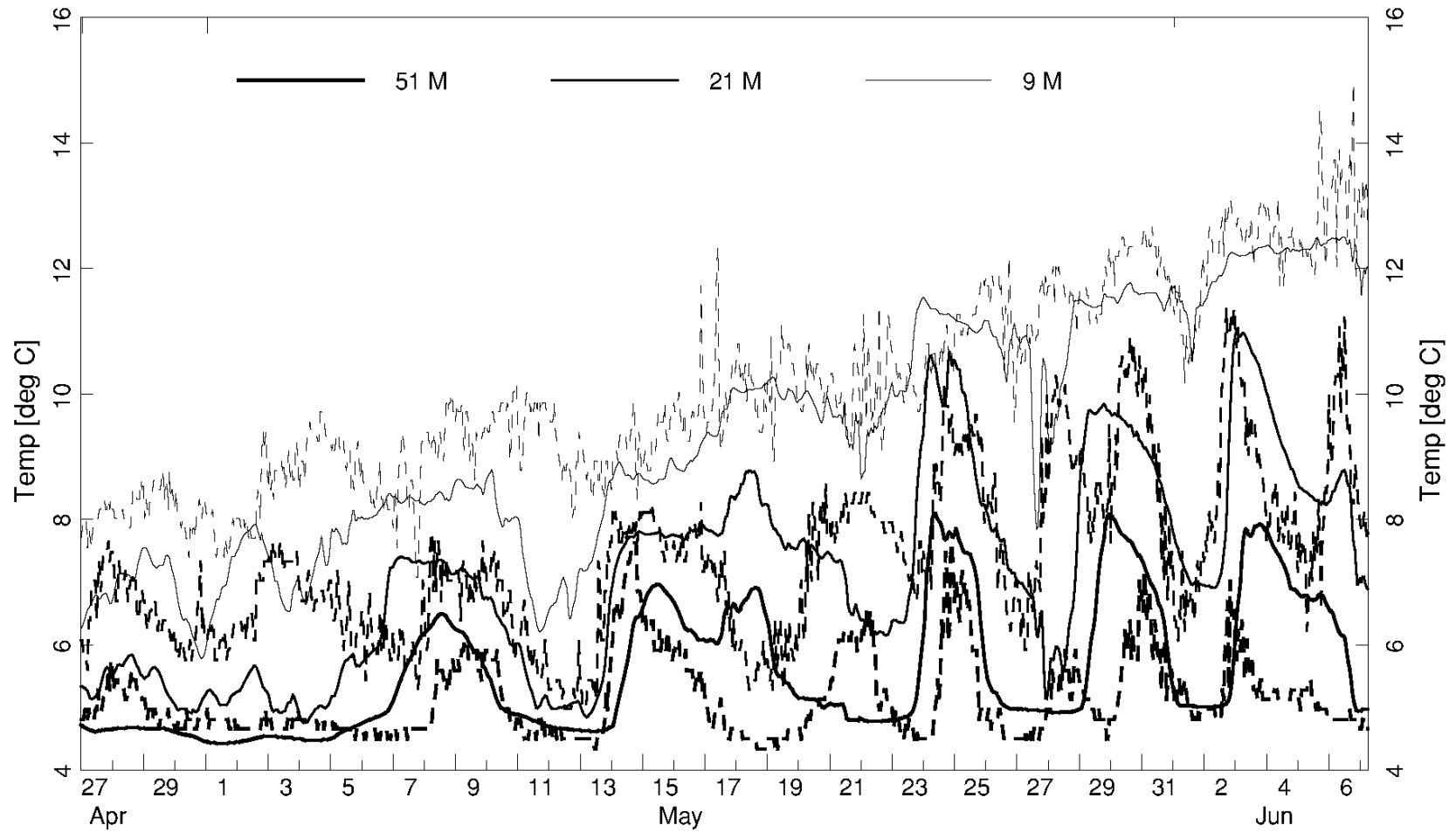
STATUS
ISSUED FOR USE



PROJECT NO. V132	DWN EW	CKD JAS	APVD JAS	REV 0
OFFICE EBA-VANC	DATE August 2, 2011			

Figure A-3

TS-A: NORTH STRING



LEGEND

Dashed Lines: Observed Temperature
 Solid Lines: Modelled Temperature

NOTES

STATUS
 ISSUED FOR USE

CLIENT



H3D TECHNICAL DESCRIPTION

H3D VALIDATION INTERNAL SEICHE DYNAMICS OKANAGAN LAKE

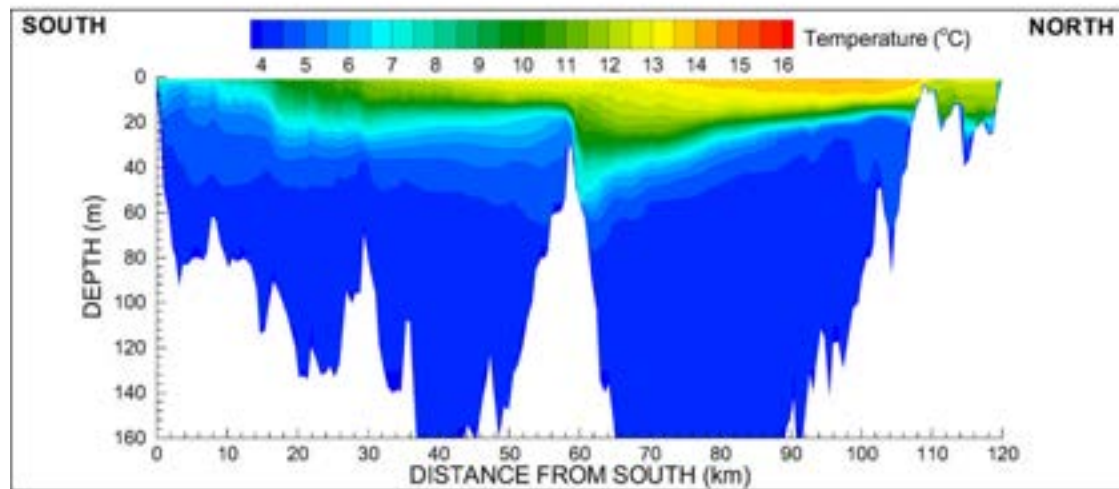
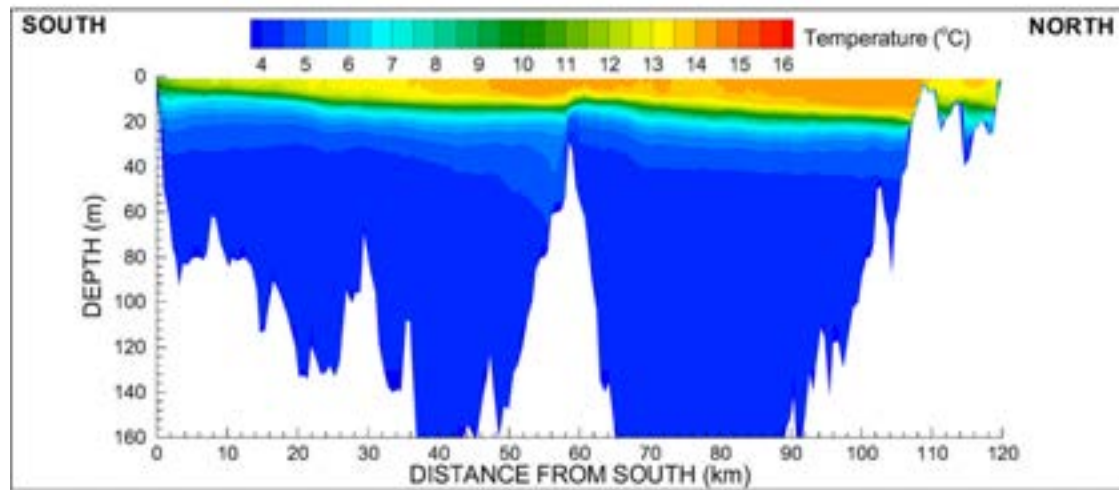
PROJECT NO.
 V132

DWN	CKD	APVD	REV
EW	JAS	JAS	0

OFFICE
 EBA-VANC

DATE
 August 2, 2011

Figure A-4



LEGEND

NOTES

CLIENT

H3D TECHNICAL DESCRIPTION

**H3D VALIDATION
INTERNAL SEICHE DYNAMICS
OKANAGAN LAKE**

STATUS
ISSUED FOR USE



PROJECT NO. V132	DWN EW	CKD JAS	APVD JAS	REV JAS
OFFICE EBA-VANC	DATE August 2, 2011			

Figure A-5

APPENDIX B

TETRA TECH EBA'S GENERAL CONDITIONS

GENERAL CONDITIONS

HYDROTECHNICAL

This report incorporates and is subject to these “General Conditions”.

1.0 USE OF REPORTS AND OWNERSHIP

This report pertains to a specific site, a specific development, and a specific scope of work. The report may include plans, drawings, profiles and other supporting documents that collectively constitute the report (the “Report”).

The Report is intended for the sole use of Tetra Tech EBA’s Client (the “Client”) as specifically identified in the Tetra Tech EBA Services Agreement or other Contract entered into with the Client (either of which is termed the “Services Agreement” herein). Tetra Tech EBA does not accept any responsibility for the accuracy of any of the data, analyses, recommendations or other contents of the Report when it is used or relied upon by any party other than the Client, unless authorized in writing by Tetra Tech EBA.

Any unauthorized use of the Report is at the sole risk of the user. Tetra Tech EBA accepts no responsibility whatsoever for any loss or damage where such loss or damage is alleged to be or, is in fact, caused by the unauthorized use of the Report.

Where Tetra Tech EBA has expressly authorized the use of the Report by a third party (an “Authorized Party”), consideration for such authorization is the Authorized Party’s acceptance of these General Conditions as well as any limitations on liability contained in the Services Agreement with the Client (all of which is collectively termed the “Limitations on Liability”). The Authorized Party should carefully review both these General Conditions and the Services Agreement prior to making any use of the Report. Any use made of the Report by an Authorized Party constitutes the Authorized Party’s express acceptance of, and agreement to, the Limitations on Liability.

The Report and any other form or type of data or documents generated by Tetra Tech EBA during the performance of the work are Tetra Tech EBA’s professional work product and shall remain the copyright property of Tetra Tech EBA.

The Report is subject to copyright and shall not be reproduced either wholly or in part without the prior, written permission of Tetra Tech EBA. Additional copies of the Report, if required, may be obtained upon request.

2.0 ALTERNATIVE REPORT FORMAT

Where Tetra Tech EBA submits both electronic file and hard copy versions of the Report or any drawings or other project-related documents and deliverables (collectively termed Tetra Tech EBA’s “Instruments of Professional Service”), only the signed and/or sealed versions shall be considered final. The original signed and/or sealed version archived by Tetra Tech EBA shall be deemed to be the original. Tetra Tech EBA will archive the original signed and/or sealed version for a maximum period of 10 years.

Both electronic file and hard copy versions of Tetra Tech EBA’s Instruments of Professional Service shall not, under any circumstances, be altered by any party except Tetra Tech EBA. Tetra Tech EBA’s Instruments of Professional Service will be used only and exactly as submitted by Tetra Tech EBA.

Electronic files submitted by Tetra Tech EBA have been prepared and submitted using specific software and hardware systems. Tetra Tech EBA makes no representation about the compatibility of these files with the Client’s current or future software and hardware systems.

3.0 STANDARD OF CARE

Services performed by Tetra Tech EBA for the Report have been conducted in accordance with the Services Agreement, in a manner consistent with the level of skill ordinarily exercised by members of the profession currently practicing under similar conditions in the jurisdiction in which the services are provided. Professional judgment has been applied in developing the conclusions and/or recommendations provided in this Report. No warranty or guarantee, express or implied, is made concerning the test results, comments, recommendations, or any other portion of the Report.

If any error or omission is detected by the Client or an Authorized Party, the error or omission must be immediately brought to the attention of Tetra Tech EBA.

4.0 ENVIRONMENTAL AND REGULATORY ISSUES

Unless expressly agreed to in the Services Agreement, Tetra Tech EBA was not retained to investigate, address or consider, and has not investigated, addressed or considered any environmental or regulatory issues associated with the project.

5.0 DISCLOSURE OF INFORMATION BY CLIENT

The Client acknowledges that it has fully cooperated with Tetra Tech EBA with respect to the provision of all available information on the past, present, and proposed conditions on the site, including historical information respecting the use of the site. The Client further acknowledges that in order for Tetra Tech EBA to properly provide the services contracted for in the Services Agreement, Tetra Tech EBA has relied upon the Client with respect to both the full disclosure and accuracy of any such information.

6.0 INFORMATION PROVIDED TO TETRA TECH EBA BY OTHERS

During the performance of the work and the preparation of this Report, Tetra Tech EBA may have relied on information provided by persons other than the Client.

While Tetra Tech EBA endeavours to verify the accuracy of such information, Tetra Tech EBA accepts no responsibility for the accuracy or the reliability of such information even where inaccurate or unreliable information impacts any recommendations, design or other deliverables and causes the Client or an Authorized Party loss or damage.

7.0 GENERAL LIMITATIONS OF REPORT

This Report is based solely on the conditions present and the data available to Tetra Tech EBA at the time the Report was prepared.

The Client, and any Authorized Party, acknowledges that the Report is based on limited data and that the conclusions, opinions, and recommendations contained in the Report are the result of the application of professional judgment to such limited data.

The Report is not applicable to any other sites, nor should it be relied upon for types of development other than those to which it refers. Any variation from the site conditions present at or the development proposed as of the date of the Report requires a supplementary investigation and assessment.

It is incumbent upon the Client and any Authorized Party, to be knowledgeable of the level of risk that has been incorporated into the project design, in consideration of the level of the hydrotechnical information that was reasonably acquired to facilitate completion of the design.

The Client acknowledges that Tetra Tech EBA is neither qualified to, nor is it making, any recommendations with respect to the purchase, sale, investment or development of the property, the decisions on which are the sole responsibility of the Client.

8.0 JOB SITE SAFETY

Tetra Tech EBA is only responsible for the activities of its employees on the job site and was not and will not be responsible for the supervision of any other persons whatsoever. The presence of Tetra Tech EBA personnel on site shall not be construed in any way to relieve the Client or any other persons on site from their responsibility for job site safety.